



Published in final edited form as:

Oncogene. 2022 January ; 41(2): 204–219. doi:10.1038/s41388-021-02085-w.

Caspase-2 regulates S-phase cell cycle events to protect from DNA damage accumulation independent of apoptosis

Ashley G. Boice^{1,2,3}, Karla E. Lopez^{1,2,3}, Raj K Pandita^{3,4}, Melissa J Parsons¹, Chloe I Charendoff^{1,2}, Vijay Charaka⁵, Alexandre F. Carisey^{2,6}, Tej K. Pandita^{3,4,5}, Lisa Bouchier-Hayes^{1,2,3}

¹Department of Pediatrics, Section of Hematology-Oncology, Baylor College of Medicine, Houston, TX 77030, USA.

²Texas Children's Hospital William T. Shearer Center for Human Immunobiology, Houston, TX 77030, USA.

³Department of Molecular and Cellular Biology, Baylor College of Medicine, Houston, TX 77030, USA.

⁴Texas A&M Institute of Biosciences and Technology, Houston, TX 77030, USA

⁵Department of Radiation Oncology, Houston Methodist Research Institute, Houston, TX 77030, USA.

⁶Department of Pediatrics, Section of Allergy and Immunology, Baylor College of Medicine, Houston, TX 77030, USA.

Abstract

In addition to its classical role in apoptosis, accumulating evidence suggests that caspase-2 has non-apoptotic functions, including regulation of cell division. Loss of caspase-2 is known to increase proliferation rates but how caspase-2 is regulating this process is currently unclear. We show that caspase-2 is activated in dividing cells in G1-phase of the cell cycle. In the absence of caspase-2, cells exhibit numerous S-phase defects including delayed exit from S-phase, defects in repair of chromosomal aberrations during S-phase, and increased DNA damage following S-phase arrest. In addition, caspase-2-deficient cells have a higher frequency of stalled replication forks, decreased DNA fiber length, and impeded progression of DNA replication tracts. This indicates that caspase-2 protects from replication stress and promotes replication fork protection to maintain genomic stability. These functions are independent of the pro-apoptotic function of caspase-2 because blocking caspase-2-induced cell death had no effect on cell division, DNA damage-induced cell cycle arrest, or DNA damage. Thus, our data supports a model where

Users may view, print, copy, and download text and data-mine the content in such documents, for the purposes of academic research, subject always to the full Conditions of use: <https://www.springernature.com/gp/open-research/policies/accepted-manuscript-terms>

*Corresponding author: **Lisa Bouchier-Hayes** bouchier@bcm.edu.

Contributions

AB, KEL, MJP, TKP and LBH conceived and designed experiments. AB, KEL, RKP, MJP, CIC, and VC performed the experiments. AFC developed the imaging analysis. AB and LBH wrote the manuscript.

Competing Interests Statement

MJP is currently employed at BD Biosciences. The remaining authors have no conflict of interest.

caspace-2 regulates cell cycle and DNA repair events to protect from the accumulation of DNA damage independently of its pro-apoptotic function.

Keywords

Caspase-2; cell cycle; apoptosis; DNA replication fork; S-phase

Introduction

Caspase-2 is a member of the caspase family of proteases that have essential roles in the initiation and execution of apoptosis.¹ Caspase-2 has been implicated in apoptosis in response to a variety of cell stressors including: DNA damage, heat shock, metabolic stress, and endoplasmic reticulum (ER) stress.² However, the requirement for caspase-2 for cell death in each of these contexts has been subject to debate.³ Despite this, caspase-2 has been shown to function as a tumor suppressor in several murine models. Caspase-2-deficient mice show accelerated tumorigenesis in murine models of hematological cancers ($E\mu$ -*Myc*-driven lymphoma⁴ and *Atm* knockout-associated lymphoma⁵), and solid tumors (*Kras*-driven lung tumors⁶ and MMTV-*c-neu*-driven mammary tumors⁷). Caspase-2-deficient tumors from these mice often show increased features of genomic instability, including aneuploidy,⁵ and cell cycle defects, such as bizarre mitoses and an increased mitotic index.⁷ Interestingly, caspase-2-deficient tumors have shown minimal differences in apoptosis compared to wild type tumors^{5, 6} suggesting that, in addition to inducing apoptosis, caspase-2 may carry out its tumor suppressive function by regulating other cellular functions such as the cell cycle.

Although it has been postulated that caspase-2 plays a role in cell cycle arrest or cell cycle checkpoint regulation,⁴ the exact phase of the cell cycle where caspase-2 primarily functions remains unclear. Caspase-2 knockout cells proliferate at higher rates.^{4, 8} In addition, caspase-2 deficiency is associated with impaired cell cycle arrest in response to DNA damage.⁴ The activation platform for caspase-2 is a large molecular weight protein complex called the PIDDosome, comprising the proteins p53-induced protein with a death domain (PIDD) and the adaptor protein RIP-associated ICH-1 homologous protein with a death domain (RAIDD).⁹ PIDD overexpression induces growth suppression that is dependent on RAIDD and partially dependent on caspase-2.^{4, 10} PIDD is a p53 target gene and PIDD can induce growth arrest in cells that are wild type for p53 but not in cells where p53 is absent or mutated.¹¹ Caspase-2 induces p53-dependent cell cycle arrest in response to supernumerary centrosomes resulting in murine double minute-2 (MDM2) cleavage and p53 stabilization.¹² Because these studies place caspase-2 upstream of p53, it is possible that caspase-2 can also regulate cell cycle in a p53-independent manner. This has been noted for caspase-2 dependent apoptosis that can be either p53-dependent¹³⁻¹⁶ or p53-independent.^{17, 18} Caspase-2 has been shown to be activated by several different inducers of DNA damage including etoposide, cisplatin, and camptothecin.^{15, 19-21} However, apoptosis can often proceed in the absence of caspase-2 in response to these triggers and, when apoptosis is reduced, it is rarely completely blocked by the absence of caspase-2.^{19, 20, 22} In particular, while caspase-2 is efficiently activated by topoisomerase I inhibitors such as camptothecin, death in response to camptothecin is only marginally, albeit significantly,

reduced in caspase-2-deficient cells.¹⁹ Of note, these drugs are also potent inducers of cell cycle arrest.^{23, 24} Inhibition of topoisomerase I triggers both cell cycle arrest and apoptosis following stalling of DNA replication forks.²⁵ Fork stalling and fork collapse results in single strand DNA (ssDNA) regions that, in the absence of repair, are converted to double-strand breaks (DSBs), serving as a trigger for cell death or cell cycle arrest.²⁶

Here, we demonstrate that, in response to replication stress, caspase-2 plays a key role in protecting from stalled replication forks and the subsequent DNA damage. Caspase-2 is activated during G1 and loss of caspase-2 is associated with several additional S-phase-related cell cycle defects including S-phase-specific chromosomal aberrations and delayed exit from S-phase following arrest. In addition, we show that these defects in cell cycle regulated events are independent of caspase-2's ability to induce apoptosis.

Materials and Methods

Chemicals and antibodies

Unless otherwise indicated antibodies were purchased from Cell Signaling Technology (Danvers, MA). The following antibodies were used: anti-caspase-2 (clone 11B4 from Millipore); anti-Geminin (Clone E5Q9S); anti-CDT1 (Clone D10F11); anti-phospho-ATM (Ser1981) (clone 10H11 from Invitrogen and clone 10H11.E12); anti-ATM (clone D2E2); polyclonal anti-phospho-ATR (Ser428); polyclonal anti-phospho-ATR (Thr1989); anti-ATR (clone E1S3S); anti-phospho-Chk1 (Ser317) (clone D12H3); anti-Chk1 (clone 2G1D5); anti-phospho-Chk2 (Thr68) (clone C13C1); anti-Chk2 (polyclonal); anti-MDM2 (clone SMP14, Sigma-Aldrich); anti-p53 (clone 1C12); anti-p21 (clone SXM30(RUO), BD Biosciences); anti-actin (C4 from MP Biomedicals); and anti- γ -H2AX (EMD Millipore). All cell culture media reagents were purchased from Thermo Fisher (Carlsbad, CA, USA). Unless otherwise indicated, all other reagents were purchased from Sigma-Aldrich (St. Louis, MO, USA).

Cell culture and cell lines

HeLa and U2OS cells were grown in Dulbecco's Modified Essential Medium (DMEM) containing FBS (10% (v/v)), L-glutamine (2 mM), and Penicillin/ Streptomycin (50 I.U./50 μ g/mL). Mouse embryonic fibroblasts (MEF) were grown in the same medium supplemented with sodium pyruvate (1 mM), 1X non-essential amino acids, and beta-mercaptoethanol (55 μ M). Litter-matched *Casp2*^{+/+} and *Casp2*^{-/-} MEF were generated and transduced with E1A and Ras as previously described.²¹ Briefly, early passage MEF were simultaneously transduced with frozen supernatants of the retroviral expression vectors pBabePuro.H-ras (G12V) and pWZLH.E1A (provided by S.W. Lowe and G. Hannon). After 48 hours, the cells were harvested by mild trypsinization, seeded at 1×10^5 cells/well in 6 well plates, and cultured for 10 days in media containing 0.5 μ g/mL of puromycin and 40 μ g/mL of hygromycin for selection of the transduced viruses. HeLa.C2-Pro BiFC cells were generated as previously described.¹⁹ HeLa.C2-Pro BiFC cells expressing Am-Cyan-Geminin and *Casp2*^{+/+} and *Casp2*^{-/-} MEF stably expressing vector or Bcl-X_L were generated by retroviral transduction. Gryphon-Ampho packaging cells were transiently transfected with Am-Cyan-Geminin (pRetroX-SG2M-Cyan vector from Takara), pLZRS, or pLZRS.Bcl-X_L

using Lipofectamine 2000 transfection reagent (Thermo Fisher) according to manufacturer's instructions. After 48 hours, virus-containing supernatants were cleared by centrifugation and incubated with HeLa.C2-Pro BiFC, *Casp2*^{+/+}, and *Casp2*^{-/-} MEF followed by selection in neomycin for pRetroX or zeocin for pLZRS vectors.

CRISPR/Cas9 gene editing

CASP2 was deleted from U2OS and HeLa cells using an adaptation of the protocol described in ref.²⁷. Protospacer sequences for each target gene were identified using the CRISPRscan scoring algorithm (www.crisprscan.org²⁸). DNA templates for sgRNAs were made by PCR using a pX459 plasmid containing the sgRNA scaffold sequence and using the following primers:

CASP2(76) sequence:

ttaatagactactataGGCGTGGGCAGTCTCATCTTgttttagagctagaatagc

CASP2(73) sequence:

ttaatagactactataGGTGTGGAGGGCGCCATCTAgtttttagagctagaatagc

universal reverse primer: AGCACCGACTCGGTGCCACT. sgRNAs were generated by *in vitro* transcription using the HiScribe T7 high yield RNA synthesis kit (New England Biolabs). Purified sgRNA (0.5 µg) was incubated with Cas9 protein (1 µg, PNA Bio) for 10 min at room temperature. HeLa or U2OS cells were electroporated with the sgRNA/Cas9 complex using the Neon transfection system (Thermo Fisher Scientific) at 1005 V, 35 ms, and two pulses. Knockout was confirmed by PCR, western blot and sequencing.

Microscopy

Cells were imaged using one of two microscope systems. The first is a spinning disk confocal microscope (Carl Zeiss MicroImaging, Thornwood, NY, USA), equipped with a CSU-X1A 5000 spinning disk unit (Yokogawa Electric Corporation, Japan), multi laser module with wavelengths of 458 nm, 488 nm, 514 nm, 561 nm, and 647 nm and an Axio Observer Z1 motorized inverted microscope equipped with a precision motorized XY stage (Zeiss). Images were acquired with a Zeiss Plan-Neofluar 40× 1.3 NA or 63× 1.4 NA objective on an Orca R2 CCD camera using Zen 2012 software (Zeiss). The second is a Leica SP8-based Gated Continuous Wave laser scanning confocal microscope (Leica Microsystems) equipped with a white-light laser, operated by Leica software. Cells were plated on dishes containing glass coverslips coated with fibronectin (Mattek Corp. Ashland, MA, USA) 24 h prior to treatment. For time-lapse experiments, media on the cells were supplemented with HEPES (20 mM) and 2-mercaptoethanol (55 µM). Cells were allowed to equilibrate to 37°C in 5% CO₂ prior to focusing on the cells in an incubation chamber set at 37°C. For the Leica system, samples were sequentially excited by a resonant scanner at 12,000 Hz using a white light laser (excitation wavelengths: 470 nm, 514 nm and 587 nm) and emitted light was collected through a HC PL APO 63x/1.47 oil objective and through a pinhole of 1.5 AU to be finally quantified by 3 HyD detectors with the following spectral gates: 475–509 nm / 520–581 nm / 593–702 nm and during an acquisition window set from 0.7 to 6 ns using time gating.

Immunofluorescence

Cells plated on dishes containing glass coverslips coated with fibronectin were washed in 3×2 mL PBS and fixed in 2% (w/v) paraformaldehyde in PBS pH 7.2 for 10 min. Cells were washed for 3×5 min in PBS followed by permeabilization in PBS, 0.15% (v/v) Triton for 10 min. Cells were blocked in FX Image-iT™ Signal Enhancer (Thermo Fisher) for 30 min and then stained with the anti- γ -H2AX antibody at a 1:100 dilution in PBS, 2% (w/v) BSA for 1 h. After washing in PBS, 2% (w/v) BSA, the cells were incubated with anti-mouse Alexa Fluor 555-conjugated secondary antibody (Thermo Fisher) at a 1:500 dilution in PBS, 2% (w/v) BSA for 45 min. Cells were washed in PBS, stained with SYTO™ 13 green fluorescent nucleic acid stain (400 nM, Thermo Fisher) in PBS and incubated at room temperature in the dark for 1 h prior to imaging.

Image analysis

At least 30 individual images were acquired for each treatment. For quantitation of nuclei, cells were stained with NucBlue™ Live ReadyProbes™ stain (a formulation of Hoechst 33342 from Thermo Fisher) and individual nuclei were counted using the python-based CellProfiler™ software (Massachusetts Institute of Technology, Broad Institute of MIT and Harvard). Greyscale TIFF images were corrected for illumination differences using an illumination function. Images were smoothed by Gaussian method followed by separation using Otsu with an adaptive thresholding strategy. Cells were then declumped by shape and automatically counted. For quantitation of γ -H2AX foci, the number of foci per cell was calculated from RGB TIFF images using FoCo, a graphical user interface that uses MATLAB (Mathworks) and ImageJ (NIH).²⁹ In the nuclei channel, Huang thresholding was used to separate cells. A Top-Hat transformation was used on foci images for noise reduction. Foci were segmented by using the threshold found by Otsu's method as minimal peak height in H-maxima transform. Foci per cell were then calculated automatically.

For analysis of time-lapse imaging, cells expressing the BiFC components were identified by fluorescence of the linked mCherry protein in stable cell lines. The raw signal from mCherry was first improved using Noise2Void³⁰ algorithm for denoising using deep learning approach. The Noise2Void 2D model was trained from scratch for 100 epochs on 148480 image patches (image dimensions: (520,520), patch size: (64,64)) with a batch size of 128 and a MSE loss function, using the Noise2Void 2D ZeroCostDL4Mic³¹ notebook (v 1.13) on Colab cloud services (Google) and then applied to all images from the mCherry channel. Next, using the same platform (Google Colab) and ZeroCostDL4Mic notebook,³¹ the CellPose algorithm³² was applied to this “enhanced” mCherry channel in order to create accurate masks of each cell (Object diameter: 20 μ m, flow threshold 0.4–0.7 and cell probability threshold 0.4–0.7 depending on the set). Raw data and CellPose masks were imported into Aivia 9.8 (Leica Microsystems) and the mean fluorescence intensity was measured in each of the Cyan and Venus channels using the CellPose-derived masks as regions of interest. After manual verification and curation of the lineage attributions, data was exported for further analysis in MATLAB (r2021a, MathWorks) where all the timelines from the different cells were aligned according to their cytokinesis time point, and were scaled by the following formula: scaled point = $(x - \text{Min})/\text{MaxDifference}$, where Min equals the minimum value in the series, x equals the point of interest, and MaxDifference equals

the maximum minus the minimum value in the series. Computer codes are available upon request.

Flow cytometry

For cell cycle analysis, cells were treated as indicated (see figure legends). Treatment media were exchanged for media containing BrdU (10 μ M). After 30 min, cells were collected by trypsinization, fixed, permeabilized, and stained with anti-BrdU-FITC antibody and 7-aminoactinomycin D (7-AAD) using the BD Pharmingen™ FITC BrdU flow kit according to the manufacturer's protocol. Briefly, the cells were fixed and permeabilized with BD Cytofix/Cytoperm buffer for 15 min at room temperature, then with the secondary permeabilization buffer, BD Cytoperm Permeabilization Buffer Plus, for 10 min on ice and finally with BD Cytofix/Cytoperm buffer for 5 min at room temperature. Cells were washed in BD Perm/Wash buffer and centrifuged at $300 \times g$ between each step. To uncover the BrdU epitope, the cells were treated with DNase (30 μ g per 10^6 cells) for 1 h at 37°C, washed in BD Perm/Wash buffer, and centrifuged at $300 \times g$. The cells were then incubated in a 1:50 dilution of FITC-labeled anti-BrdU antibody in BD Perm/Wash buffer for 20 min at room temperature, washed and centrifuged at $300 \times g$. The cells were then resuspended in Stain Buffer (3% FBS in PBS) containing 10 μ L of 7-AAD/ 10^6 cells. Cells were quantitated for BrdU and 7-AAD positivity by flow cytometry. For Annexin V binding, cells were resuspended in 200 μ L of Annexin V binding buffer (10 mM HEPES, 150 mM NaCl, 5 mM KCl, 1 mM MgCl₂, and 1.8 mM CaCl₂) supplemented with 2 μ L of Annexin V-FITC (Caltag Laboratories, Burlingame, CA). Annexin V-positive cells were quantitated by flow cytometry.

Cell cycle synchronization

For synchronization of HeLa cells at G2, 2.5×10^5 cells were treated with 2 mM thymidine for 18 h. The cells were then washed twice with PBS, and fresh media was added. After incubating the cells for 9 h, they were treated with 2 mM thymidine for a further 24 h. The cells were washed with PBS twice and recovered for 2 h in growth media. The cells were then treated with the cyclin dependent kinase 1 (CDK1) inhibitor Ro-3306 (10 μ M) for 12 h. The cells were washed twice with PBS and fresh media was added. The cells were harvested every hour for 10 h.

Immunoblotting

Cell lysates were resolved by SDS-PAGE. The proteins were transferred to nitrocellulose (Thermo Fisher) and immunodetected using appropriate primary and peroxidase-coupled secondary antibodies (Genesee Scientific). Proteins were visualized by West Pico and West Dura Chemiluminescence Substrate (Thermo Fisher).

DNA fiber analysis

Exponentially growing cells were pulse-labeled with 50 mM 5-chlorodeoxyuridine (CldU) for 30 min, washed three times with PBS, treated with 2 mM hydroxyurea (HU) for 2 h, washed three times with PBS, incubated again in fresh medium containing 50 mM 5-iododeoxyuridine (IdU) for 60 min, and then washed three times in PBS. DNA fiber

spreads were made by a modification of a procedure described previously.³³ Briefly, cells labeled with IdU and CldU were mixed with unlabeled cells at a ratio of 1:10, and 2 μ L cell suspensions were dropped onto a glass slide and then mixed with 20 μ L hypotonic lysis solution (10 mM Tris-HCl [pH 7.4], 2.5 mM MgCl₂, 1 mM phenylmethylsulfonyl fluoride [PMSF], and 0.5% Nonidet P-40) for 8 min. Air-dried slides were fixed, washed with 1 \times PBS, blocked with 5% BSA for 15 min, and incubated with primary antibodies against IdU and CldU (rat anti-IdU monoclonal antibody [MAb] [1:150 dilution; Abcam] and mouse anti-CldU MAb [1:150 dilution; BD]) and secondary antibodies (anti-rat Alexa Fluor 488-conjugated [1:150 dilution] and anti-mouse Alexa Fluor 568-conjugated [1:200 dilution] antibodies [Thermo Fisher]) for 1 h each. Slides were washed with 1x PBS with 0.1% Triton X-100 and mounted with Vectashield mounting medium without 4', 6-diamidino-2-phenylindole (DAPI). ImageJ software (NIH) was used to analyze the DNA fibers. For each data set, about 300 fibers were counted for stalled forks, new origins, or elongated forks.

Viability assay

Casp2^{+/+} and *Casp2^{-/-}* MEF were plated in a 6-well or 12-well plate at the indicated densities. After 4 days, colonies were visualized by staining overnight with methylene blue 0.1% w/v in methanol/water 50% v/v at room temperature. Cells were washed in PBS.

Assay for chromosomal aberrations at metaphase

All three stage-specific chromosomal aberrations were analyzed at metaphase after exposure to irradiation (IR). G1-type chromosomal aberrations were assessed in cells exposed to 3 Gy of IR and incubated for 10 h and metaphases were collected.^{34, 35} S-phase-specific chromosome aberrations were assessed after exponentially growing cells were irradiated with 2 Gy of IR. S-phase types of chromosomal aberrations were scored in metaphases harvested 4 h following irradiation. For G2-specific aberrations, cells were irradiated with 1 Gy and metaphases were collected 1 h post treatment. Chromosome spreads were prepared after hypotonic treatment of cells, fixed in acetic acid/methanol (1:3), and stained with Giemsa. The categories of G1-type asymmetrical chromosome aberrations that were scored include dicentrics, centric rings, interstitial deletions/acentric rings, and terminal deletions. S-phase chromosome aberrations were assessed by counting both the chromosome and chromatid aberrations, including triradial and quadriradial exchanges per metaphase as previously described.^{34, 35} G2-phase chromosomal aberrations were assessed by counting chromatid breaks and gaps per metaphase as previously described.^{34, 35} Fifty metaphases were scored for each post-irradiation time point.

Statistical analysis

Statistical comparisons were performed using two-tailed Student's t test or unpaired t test using Holm-Sidak method to correct for multiple comparisons calculated using Prism 7.03 (Graph Pad) software.

Results

Loss of caspase-2 increases cell growth

Loss of caspase-2 has been previously shown to increase cellular proliferation rates.^{4, 8} To confirm, we plated E1A/Ras-transformed litter-matched *Casp2*^{+/+} and *Casp2*^{-/-} mouse embryonic fibroblasts (MEF) at low densities and stained for viable cells after 4 days. *Casp2*^{-/-} MEF consistently exhibited an increase in the number of colonies compared to *Casp2*^{+/+} cells (Figure 1A). We used CRISPR/Cas9 to generate human caspase-2-deficient HeLa cells (HeLa C2) and we noted a similar proliferative advantage in the absence of caspase-2 (Figure 1B). We compared the growth rates of *Casp2*^{+/+} and *Casp2*^{-/-} cells. Caspase-2-deficient cells demonstrated increased proliferation 72 h following plating (Figure 1C, D). To confirm these results, we used BrdU/7-AAD staining to determine the cell cycle profiles of cycling *Casp2*^{+/+} and *Casp2*^{-/-} MEF and found that *Casp2*^{-/-} cells had significantly more cells in S-phase and less cells in G1-phase compared to the *Casp2*^{+/+} cells (Figure 1E, F). The increased proportion of S-phase cells suggests more caspase-2-deficient cells are synthesizing DNA, while the reduced G1 cells indicate that a decreased proportion of the *Casp2*^{-/-} cells are in a quiescent state compared to *Casp2*^{+/+} cells. This is consistent with the higher rate of proliferation we observed for caspase-2-deficient cells. Together, these results indicate that caspase-2 plays a role in limiting uncontrolled cell growth.

Because caspase-2 appears to be involved in regulating cell proliferation, we hypothesized that caspase-2 is activated in cells undergoing mitosis. To investigate this, we used the caspase-2 bimolecular fluorescence complementation (BiFC) technique.²¹ This technique relies on the fact that caspase-2 is activated by proximity-induced dimerization following recruitment to its activation platform.^{9, 36} Caspase-2 BiFC uses non-fluorescent fragments of the fluorescent protein Venus fused to the prodomain of caspase-2.²¹ When caspase-2 is recruited to its activation platform the subsequent induced proximity of caspase monomers enforces refolding of the Venus fragments, reconstituting their fluorescence. We used the HeLa.C2 Pro-BiFC line, which stably expresses the caspase-2 BiFC reporter comprising of the prodomain of caspase-2 (aa 1–147) fused to the Venus fragments, Venus N 1–173 (VN) or Venus C 155–249 (VC) separated by the virally derived 2A self-cleaving peptide to ensure equal expression of the BiFC components.¹⁹ The C2-Pro BiFC sequence is also linked to a mCherry sequence to permit visualization of the cells. We used time-lapse confocal microscopy to track caspase-2 BiFC relative to cell division in unstimulated cells. We used the mCherry signal, which fluoresces throughout the cell, to visualize cell division (Figure 2A). Caspase-2 BiFC (Venus) peaked around the time of mitosis as a series of cytoplasmic puncta that disappeared over time. This occurred in the majority of cells undergoing cell division (Figure 2A, 2B, Supplemental Movie S1). In contrast, in cells that did not divide or in cells that died during the course of the time-lapse, the proportion of cells inducing caspase-2 BiFC was equal to the proportion of cells that remained BiFC-negative. Based on cell morphology, it is likely that many of the BiFC-positive cells with no observed division underwent division immediately before or after the time-lapse window, accounting for the wide range in this group between experiments (16–71%) compared to the other groups. These results show that caspase-2 is activated in dividing cells around the time of mitosis.

To track cell division and the timing of caspase-2 BiFC relative to the cell cycle more accurately, we monitored caspase-2 BiFC relative to a stably expressed fluorescent cell cycle marker, AmCyan-hGeminin. hGeminin is only expressed in S and G2/M-phase of the cell cycle,³⁷ therefore fluorescence of AmCyan-hGeminin is most concentrated in G2 and is degraded in early G1.³⁸ During the time-lapse the majority of cells underwent at least two rounds of cell division and, thus, we were able to observe at least two peaks of geminin activation for each cell. When we analyzed the cells that induced caspase-2 BiFC during division, the peak of caspase-2 fluorescence averaged across all cell divisions was detected 160 min following the peak of the AmCyan-hGeminin signal (Figure 2C, 2D, Supplemental Movie S2). This indicates that caspase-2 activation does not coincide G2/M phase of the cell cycle but is activated in G1-phase.

To confirm that the results with the fluorescent reporter for caspase-2 activation were indicative of the behavior of the endogenous protein we measured caspase-2 cleavage in relation to the different phases of the cell cycle. We synchronized the cells at G2 using double thymidine block followed by CDK1 inhibition. Geminin expression decreased 6 h following removal of the CDK1 inhibitor, which was accompanied by an increase in CDT1 expression, which is stabilized in G1 and degraded at the onset of S-phase.³⁹ Caspase-2 cleavage was determined by the appearance of the intermediate cleavage fragment at 2 h and the p20 catalytic subunit that started at 5 h and peaked at 7 h (Figure 2E). The peak level of fully processed caspase-2 was detected 2 h following the peak geminin signal, which confirms the time difference between the hGeminin peak and caspase-2 activation recorded in the imaging studies. Together, these data indicate that caspase-2 is activated during the G1-phase of the cell cycle

Loss of caspase-2 results in delayed exit from S-Phase

The activation of caspase-2 in G1 and the specific increase in cells in S-phase in the absence of caspase-2 suggests a role for caspase-2 in ensuring normal G1 or S-phase progression. Therefore, we investigated the impact of loss of caspase-2 on cell cycle recovery after G1/S-phase arrest. We treated *Casp2*^{+/+} and *Casp2*^{-/-} MEF with aphidicolin for 16 h to synchronize the cells. As expected, aphidicolin arrested the *Casp2*^{+/+} MEF in S-phase and at the G1/S border (Figure 3A, 0 h). In contrast, immediately after release from S-phase arrest (0 h), there was a greater proportion of *Casp2*^{-/-} MEF in S-phase compared to *Casp2*^{+/+} MEF and an increase in G2 cells (Figure 3A, B). This indicates that aphidicolin arrests the cells more in S and G2 phase in the absence of caspase-2 rather than on the G1/S border. In addition, over four hours following release from arrest, the proportion of *Casp2*^{+/+} MEF in S-phase reduced as the cells moved into G2 and then G1. In contrast, *Casp2*^{-/-} cells exhibited a delay in exit from S-phase and concomitant entry into G1 (Figure 3A, B). To confirm these results, we carried out a similar experiment in HeLa cells with or without caspase-2 (Figure 3C, D). We arrested the cells with L-mimosine, which similarly arrests cells on the G1/S border. The wild-type cells arrested in late G1 and early S-phase as expected. In contrast, the caspase-2-deficient cells arrested more in G1. The caspase-2-deficient cells then moved into S-phase but did not appear to transition as quickly into G2. Rather, they remained in S and on the S/G2 border. In contrast, by 4 h, the wild-type cells had formed a distinct G2 population and started to progress to G1, as determined by the

increase in the proportion of cells in G1-phase. In the absence of caspase-2, we noted a steady decline in G1 cells following arrest but no change in G2. These results indicate that the entry into S-phase is unaffected by the absence of caspase-2 but the exit from S-phase is delayed.

Caspase-2 protects from stalled replication forks and replication stress

The delayed recovery from S-phase arrest we observed in *Casp2*^{-/-} cells could be due to DNA replication stress. Therefore, we investigated the role of caspase-2 in replication fork dynamics following transient genotoxic stress-induced replication blockage. We used a DNA fiber assay to evaluate restart and recovery of replication forks after hydroxyurea (HU) treatment. HU induces replication fork stalling and S-phase arrest by depleting the available nucleotide pool for DNA polymerases.⁴⁰ Cells were pulse-labeled with 5-chlorodeoxyuridine (CldU), treated with HU for 2 h to induce replicative stress, and then washed and pulse-labeled with 5-iododeoxyuridine (IdU). Individual DNA fibers, which incorporated the CldU and/or IdU pulses, were detected with fluorescent antibodies against those thymidine analogs (Figure 4A, B). We noted three types of DNA fiber tracts: those with ongoing elongation forks (CldU+IdU), stalled forks (CldU), and newly initiated forks (IdU) representing new origins of DNA replication. Caspase-2-deficient MEF demonstrated a significantly higher frequency of stalled replication forks (Figure 4C), new origins of replication (Figure 4D), and a reduced frequency of CldU+IdU forks, indicating reduced ongoing replication (Figure 4E). Caspase-2-deficient HeLa similarly showed a significantly higher frequency of stalled replication forks (Figure 4F), and a reduced frequency of CldU+IdU forks (Figure 4G). This suggests that the loss of caspase-2 prevents or delays re-initiation of stalled replication forks that can result in S-phase arrest, while also resulting in excessive replication-origin firing. When replication is stalled, the length of DNA tract is impacted.⁴¹ Therefore, to assess the impact of caspase-2 loss on DNA tract length, we measure the length of the total tract of CldU + IdU and the length of CldU or IdU labeled DNA fibers in *Casp2*^{+/+} and *Casp2*^{-/-} cells, and in HeLa^{WT} and HeLa C2 cells. As expected, the length of the CldU fibers, which represents the DNA prior to replication stress, were the same across the cell types. The length of IdU was significantly reduced in caspase-2-deficient MEF and HeLa compared to wild type (Figure 4H, I). This reduced fiber length indicates a reduced DNA fork speed and, thus, increased replication stress in the absence of caspase-2. Thus caspase-2 promotes replication fork progression.

Loss of caspase-2 is associated with DNA damage and impaired DNA repair

Excessive replication fork stalling induced by HU treatment can lead to fork collapse and breakage in the form of DSBs.^{26, 42} To probe the effects of loss of caspase-2 on DSBs induced by replication stress, we stained for phosphorylated H2AX (γ -H2AX). γ -H2AX forms foci at DSBs and therefore is a reliable and sensitive indicator of DSBs.⁴³ We treated *Casp2*^{+/+} and *Casp2*^{-/-} MEF with HU for 2 h and quantitated the percentage of cells with γ -H2AX foci 24 h later. We observed a significantly higher level of cells with γ -H2AX foci in *Casp2*^{-/-} MEF compared to the wild-type MEF (Figure 5A, B). These data indicate a higher level of DNA damage following replication stress in the absence of caspase-2. This suggests that caspase-2 functions to prevent DNA damage or to facilitate DNA repair.

Next, we determined if DNA repair is affected by the presence or absence of caspase-2. We examined cell cycle-phase specific chromosomal aberrations at metaphase induced by different doses of ionizing irradiation (IR). The different doses induce damage at these stages with minimum effect on the mitotic index. The cells in exponential phase were irradiated and grown for specific times that it takes to reach metaphase. G1-specific chromosome aberrations were analyzed in cells treated with 3 Gy and metaphases were collected 10 h post irradiation. S-specific chromosome aberrations were analyzed in cells treated with 2 Gy and metaphases were collected 4 h post irradiation and G2-specific chromosome aberrations were analyzed in cells treated with 1 Gy and metaphases were collected 1 h post irradiation. The frequency of G1-type chromosomal aberrations (mostly of the chromosomal type with frequent dicentric chromosomes)⁴⁴ and G2-type chromosomal aberrations (chromosomal and chromatids) was similar for *Casp2*^{+/+} and *Casp2*^{-/-} cells (Figure 5C). In contrast, S-type aberrations were specifically increased in *Casp2*^{-/-} cells. These aberrations consisted primarily of breaks and radials (Figure 5D). The lack of differences in G1-induced or G2-induced chromosomal aberrations seen at metaphase between *Casp2*^{+/+} and *Casp2*^{-/-} cells indicate normal G1 and G2 checkpoints respectively. The difference in S-phase-induced chromosomal aberrations indicate that this damage is not repaired efficiently before onset of mitosis in these cells. In S-phase, homologous recombination (HR) repair is the predominant mode of DNA repair, indicating that caspase-2 is involved in HR.

Loss of caspase-2 has minimal impact on the canonical intra S-phase checkpoint

Stalled replication forks lead to activation of ATR and its substrate Chk1.⁴⁵ Chk1 triggers a G2/M checkpoint by inhibiting Cdc25C-mediated activation of Cyclin B⁴⁶ and also triggers an intra S-phase checkpoint through inhibition of Cdc25A-mediated activation of Cyclin A/E.⁴⁷ Given the increase in stalled forks and delayed exit from S-phase in the absence of caspase-2, we measured the impact of loss of caspase-2 on ATR and Chk1 activation. To measure checkpoint activation, we treated *Casp2*^{+/+} and *Casp2*^{-/-} MEF with HU for 2 h to stall the cells in S-phase and upregulate S-phase-associated checkpoint proteins (0 h). Upon removal of the drug, cells go back into cycle and the checkpoint proteins are expected to be dephosphorylated over time (2–4 h) (Figure 6A). As expected, Chk1 was phosphorylated immediately after the removal of HU, indicating activation of the intra-S checkpoint, and began to decrease over the 4 h as cells began to cycle again (Figure 6B). Chk1 was phosphorylated to a similar extent in cells with and without caspase-2 and minimal differences in Chk1 phosphorylation between the two cell lines were noted over time. Interestingly, phosphorylation of ATR increased 2 h following HU release in *Casp2*^{+/+} MEF and this was inhibited in *Casp2*^{-/-} MEF. However, the phosphorylation that was detected was at Serine 428. Phosphorylation of ATR at this site is not required for Chk1 phosphorylation and therefore is not associated with canonical ATR activation.⁴⁸ Because antibodies for the phospho-ATR site that is associated with activation (threonine 1989) are not available for murine ATR, we used CRISPR/Cas9 to generate human caspase-2-deficient U2OS cells to determine if caspase-2 is required for ATR activation. As in the MEF, loss of caspase-2 had no effect on Chk1 phosphorylation induced by two different doses of HU or the DNA damage inducers: etoposide, camptothecin or topotecan (Figure 6C). Phosphorylation of ATR at T1989 was not substantially impacted by the loss of caspase-2

under any of the treatment conditions. We also tested this in HeLa cells and no difference in Chk1 phosphorylation was observed with or without caspase-2 (Figure 6D). Finally, we examined Chk1 phosphorylation in response to S-phase arrest induced by aphidicolin in U2OS cells (Figure 6E). Following release from aphidicolin, we did not detect any difference in Chk1 phosphorylation.

ATM regulates the intra-S phase checkpoint through Chk2 activation.⁴⁹ Similar to ATR, we saw some induction of ATM phosphorylation in MEF 2 h following removal of HU (Figure 6B). This phosphorylation was detected earlier in *Casp2*^{-/-} MEF and was diminished by 2 h. However, the phosphorylation of ATM was not accompanied by phosphorylation of the ATM substrate, Chk2.⁵⁰ In MEF, Chk2 phosphorylation was detected at the later 4 h time-point. This appeared caspase-2-dependent, but it was not consistent across experiments. ATM is activated primarily by double strand breaks.⁵¹ To determine the effect of loss of caspase-2 on ATM activation in response to DSBs, we measured ATM and Chk2 phosphorylation in response to etoposide compared to the single strand DNA break inducers, camptothecin and topotecan, and to HU in U2OS cells (Figure 6C). We observed strong phosphorylation of Chk2 immediately after release from etoposide, camptothecin, or topotecan in the presence and absence of caspase-2. In contrast, HU did not induce much Chk2 phosphorylation. In response to etoposide and topotecan, phosphorylated ATM was maximal at 2 h in wild-type cells and, although diminished, the peak of phosphorylation was 0 h in knockout cells. In response to camptothecin, the ATM phosphorylation peak was detected in caspase-2-deficient cells at 2 h and was not detected in wild-type cells. This indicates that ATM phosphorylation and dephosphorylation is accelerated in the absence of caspase-2. ATM phosphorylation was not induced by HU in the U2OS cells. In HeLa cells and in U2OS cells, we detected strong Chk2 phosphorylation in response to HU and aphidicolin, respectively in the presence and absence of caspase-2 (Figure 6D and E). Taken together, these results suggest that caspase-2 is either activated downstream of ATM/Chk2 and ATR/Chk1 or in parallel to these checkpoints.

p53 is activated downstream of both ATM and ATR. In addition, the p53 target gene MDM2 is a known caspase-2 substrate. Cleavage of MDM2 by caspase-2 leads to increased p53 stabilization.¹¹ We measured p53 stabilization and MDM2 cleavage in the presence and absence of caspase-2. As we previously reported,⁷ we noted an increased basal level of p53 in caspase-2-deficient MEF but this did not increase as much as in *Casp2*^{+/+} cells following treatment (Figure 6F). In U2OS cells, there was a small decrease in p53 in the absence of caspase-2 in response to all treatments (Figure 6G). However, the small changes in p53 levels in either cell line were not accompanied by a difference in expression of the p53 target, p21, indicating that p53 function is intact under these conditions in the absence of caspase-2 (Figure 6F, G). MDM2 cleavage was observed in a caspase-2-dependent manner in response to treatment with the Aurora B kinase inhibitor ZM447439 but was notably absent in response to the DNA damage stimuli or HU in MEF and U2OS (Figure 6F, G). These results indicate that caspase-2 has minimal impact on p53 function and does not induce MDM2 cleavage in response to replication stress.

Caspase-2 induced cell cycle regulation is independent from its ability to induce apoptosis

Caspase-2 induces apoptosis through cleavage of the pro-apoptotic protein BID and subsequent permeabilization of the outer mitochondrial membrane, cytochrome c release, and downstream caspase activation.^{52, 53} However, it is unclear if the pathway engaged by caspase-2 to regulate the cell cycle is the same pathway that induces apoptosis. To investigate this, we overexpressed Bcl-X_L in *Casp2*^{+/+} and *Casp2*^{-/-} MEF. We treated *Casp2*^{+/+} and *Casp2*^{-/-} MEF expressing vector or Bcl-X_L with a range of doses of camptothecin for 24 h. We previously reported that *Casp2*^{-/-} MEF were less sensitive to apoptosis induced by exposure 250 nM camptothecin for 16 h.¹⁹ Here, we noted a small but significant decrease in apoptosis without caspase-2 only at the 100 nM dose after a longer 24 h incubation (Figure 7A). This resistance was lost at higher doses of camptothecin. This difference in sensitivity from our prior study is likely due to the increased incubation time with the drug. Bcl-X_L overexpressing *Casp2*^{+/+} and *Casp2*^{-/-} MEF were profoundly resistant to camptothecin-induced apoptosis (Figure 7A). The cell cycle profile of untreated Bcl-X_L-overexpressing *Casp2*^{+/+} cells was unchanged compared to that of the vector-transduced *Casp2*^{+/+} MEF (Figure 7B). This suggests that the association between the increased frequency of S-phase defects and loss of caspase-2 is not due to apoptosis induced by caspase-2, indicating that a distinct pathway is engaged to induce the observed cell cycle-related effects. To explore this further, we treated *Casp2*^{+/+} and *Casp2*^{-/-} MEF expressing vector or Bcl-X_L with camptothecin for 4 h and measured cell cycle arrest at 4 h and apoptosis at 24 h (Figure 7B). These treatment conditions (4 h exposure to camptothecin followed by complete growth medium) induced minimal apoptosis after 24 h that was blocked by overexpression of Bcl-X_L (Figure 7B). When we challenged the cells with low doses of camptothecin, *Casp2*^{+/+} cells accumulated in S-phase and this was increased in *Casp2*^{-/-} cells. At higher doses of camptothecin, *Casp2*^{+/+} cells accumulated more in G2/M-phase. This was slightly increased in the absence of caspase-2, but the effect was variable and not significant. The proportions of G1 cells steadily decreased with increasing dose of camptothecin. The increases in S-phase arrest at lower doses, G2-arrest at high doses, and decreased G1 cells in the absence of caspase-2 was not changed by the overexpression of Bcl-X_L (Figure 7B). In addition, DNA damage, as measured by γ -H2AX staining following HU treatment, was not increased in cells overexpressing Bcl-X_L, while it was in the absence of caspase-2 regardless of the presence or absence of Bcl-X_L (Figure 7C). Together these results indicate that the S-phase defects and increased susceptibility to DNA damage associated with caspase-2 deficiency are independent of the ability of caspase-2 to induce apoptosis.

Loss of caspase-2 leads to faster recovery from mild DNA damage

Our data so far indicates that caspase-2 is important for DNA repair and without caspase-2, the checkpoint required for DNA repair is bypassed leading to faster proliferation rates and propagation of that damage. To test this, we used CRISPR/Cas9 to delete caspase-2 in the HeLa.C2-ProBiFC-AmCyan-hGeminin cells to determine the impact of mild DNA damage on cell cycle length in the presence and absence of endogenous caspase-2 (Figure 8A). In the absence of caspase-2, cells should still be able to induce caspase-2 BiFC because all the upstream elements are present. However, the reporter is not enzymatic, therefore all downstream, caspase-2-dependent events should be inhibited. We treated the cells with

a range of concentrations of camptothecin to identify a dose that would impair but not inhibit cell cycle (Figure 8B). As expected, in viable cells that became positive for caspase-2 BiFC over the period of the time-lapse, we observed more cell divisions in the absence of caspase-2 compared to wild-type cells. In cells treated with 2.5 nM camptothecin, cell division was not impaired, but again there were increased numbers of complete divisions in the absence of caspase-2. We also noted that more cells underwent three generations of division in caspase-2-deficient cells treated with 2.5 nM of camptothecin. At increased doses, there was minimal division that did not result in cell death with or without caspase-2. Using 2.5 nM camptothecin as a sub-lethal dose of DNA damage, we tracked cell division in single cells and the changes in intensity of the AmCyan-hGeminin and the C2-Pro BiFC signals representing cell division and caspase-2 activation respectively. We compared the time between sequential peaks of hGeminin signal, representing a completed cycle (Figure 8C), in each cell and followed the changes in fluorescence of all the cells in the population over time (Figure 8D, E). To focus on the impact of caspase-2 on cell division in the absence of cell death, we excluded cells that did not undergo two sequential rounds of cell division, cells that died, and those that did not activate caspase-2. Upon treatment, the average cycle length of wild type cells increased by 2 h, likely to accommodate DNA repair (Figure 8C). The cell cycle length was also increased in unstimulated caspase-2 deficient cells compared to wild type cells, (Figure 8C, D) but this was probably due to slowed cycling in later generations due to overcrowding as there was increased proliferation in these cells (Figure 8B, E). Following mild camptothecin treatment of caspase-2-deficient cells, there was not a significant increase in the average cell cycle length compared to untreated wild-type cells (Figure 8C). In addition, the onset of the increase in Am-Cyan-hGeminin fluorescence following the first round of division was accelerated by 1 h 20 min and fluorescence started to decrease approximately 1 h 30 min earlier compared to wild-type stimulated cells (Figure 8D). This indicates that caspase-2-deficient cells recover faster from DNA damage and may bypass the repair. Consistent with this, there were many more cells at the end of the time-lapse in the caspase-2-deficient cells compared to the treated wild-type cells (Figure 8E, Supplemental Movie S3). Interestingly, we also observed an acceleration of caspase-2 BiFC with camptothecin treatment -- the peak Venus signal occurred more closely to the decrease of the Am-Cyan-hGeminin signal (Figure 8D). This acceleration in caspase-2 activation was dependent upon endogenous caspase-2 since the effect was not observed in caspase-2-deficient cells. Thus, these data suggest that the acceleration of caspase-2 activation in the G1-phase of the cell cycle requires caspase-2 itself.

Discussion

Here we report that caspase-2 is activated during cell division and loss of caspase-2 is associated with S-phase-specific defects, including DNA fork stalling, delayed exit from S-phase, and S-phase-specific chromosomal aberrations. These functions are independent of caspase-2's ability to induce apoptosis. Altogether, our results demonstrate that caspase-2 plays a key non-apoptotic role in the regulation of DNA replication and repair to protect against genomic instability.

Our data show that caspase-2 is activated during cell division. Notably, this activation occurred during G1 and more caspase-2-deficient cells accumulated in S-phase following

G1/S arrest than cells with wild-type caspase-2. Following S-phase arrest, cells progress through S-phase to G2 and G1 more quickly than when caspase-2 is absent. Thus, in the absence of caspase-2, cells struggle to exit S-phase, underscoring the important role of caspase-2 in S-phase of the cell cycle. During S-phase of the cell cycle, the genome of the cell is duplicated.⁵⁴ Any errors sustained during this process can manifest as replication stress resulting in stalled or collapsed replication forks.⁵⁵ Our data show that caspase-2 protects against stalled replication forks and against excessive replication-origin firing induced by replication stress. Stalled replication forks produce single strand DNA that, when collapsed, can be converted to DSBs, the accumulation of which promotes genomic instability.⁵⁶ Excessive replication origin firing leads to the depletion of necessary nutrients and metabolites required for correct genome replication, again contributing to genomic instability.^{57, 58} Several groups, including our own, have provided evidence that caspase-2 protects against genomic instability.^{5, 7, 12, 59} Loss of caspase-2 has been shown to be associated with higher levels of aneuploidy,^{59, 60} polyploidy,¹² and genome duplication.⁷ Our data showing increased DNA damage, failure to repair S-phase-associated chromosomal damage, and accelerated recovery of cell division following mild DNA damage in the absence of caspase-2 support an active role for caspase-2 in facilitating DNA repair. We propose that caspase-2 prevents genomic instability by protecting DNA replication forks during the S-phase of the cell cycle, preventing fork collapse, the resulting DNA damage and allowing for correct DNA repair to take place by activating a cell cycle checkpoint.

The canonical S-phase-associated cell cycle checkpoint is the intra-S-phase checkpoint that is required to ensure genomic integrity and to prevent errors during DNA replication.⁶¹ ATR is a critical mediator of the intra-S-phase checkpoint and is activated by ssDNA and DSBs. Several studies indicate that the complex between replication protein A and ssDNA is the convergence point for different types of lesions to activate ATR.^{46, 62} In contrast, DSBs activate ATM.^{51, 63} Surprisingly, although loss of caspase-2 was associated with increased stalled replication forks, it had minimal effects on Chk1 phosphorylation. This would suggest that caspase-2 functions downstream of, or independently of, Chk1 in response to stalled replication forks. Stalled replication forks induce excessive origin firing, which is usually repressed by ATR and Chk1.⁶⁴ The increase in new origins in the absence of caspase-2 is further evidence of disruption of this pathway. Finally, we show that loss of caspase-2 is associated with impaired HR, a pathway that repairs double strand breaks, which is also regulated by ATR.⁶⁵ Together, these results strongly support a role for ATR in caspase-2-mediated DNA repair, despite the intact Chk1 activation in the absence of caspase-2. We did observe an impairment in phosphorylation of the S428 site of ATR in the absence of caspase-2. This site is not associated with Chk1 activation⁴⁸ but could indicate an additional downstream substrate for ATR that contributes to the intra-S-phase checkpoint in a caspase-2-dependent manner. Among its many substrates, ATR phosphorylates the helicase SMARCAL1 to limit DNA replication fork collapse⁶⁶ and can also phosphorylate FANCI to promote repair of DNA interstrand crosslinks.⁶⁷ It will be important to determine if the activation these and other substrates of ATR are impaired in the absence of caspase-2.

The observed acceleration of ATM autophosphorylation/dephosphorylation in the absence of caspase-2 suggests impaired kinetics of ATM activation that could also deregulate the intra S-phase checkpoint.⁶⁸ However, this decrease was not accompanied by a change in

activation of its substrate Chk2. ATM also phosphorylates p53,⁶⁹ but we did not observe a caspase-2-dependent effect on p53 function in this context. It is possible that loss of caspase-2 has an impact on a different ATM substrate such as BRCA1⁷⁰ or NBS1⁷¹ to impact this or other checkpoints. In addition, it has been demonstrated that Chk2 can be activated independently of ATM in response to HU treatment.⁷²⁻⁷⁴ The fact that loss of caspase-2 potentiates tumorigenesis and genomic instability in an ATM-deficient background⁵ argues against any interdependence of these two pathways and suggests rather that caspase-2 and ATM function in parallel to protect against genomic instability. It is also possible that the ATM pathway is accelerated to compensate for an impairment in ATR signaling or related DNA repair pathways in the absence of caspase-2.

The excessive origin firing of caspase-2-deficient cells explains their higher proliferation rates despite the increase in stalled forks. We also observed that caspase-2-deficiency results in reduced replication fork speed, which is correlated with increased replication origin firing.⁷⁵ Caspase-2 activation following exit from G2 in response to low levels of DNA damage is accompanied by a caspase-2-dependent lengthening of the time the cell takes to complete a full cycle. Thus, mild DNA damage or replicative stress induces caspase-2 activation immediately after mitosis, which, in turn, results in restarting of stalled replication forks and suppression of new origins of replication, ensuring correct progression of cell division. This is likely the result of caspase-2-mediated cleavage of a substrate or substrates, that kinetically do not exert functional effects until S-phase. Cells with irreparable damage exit the cycle either by apoptosis or stalled division. However, in the absence of caspase-2 the stalled forks are not resolved, prolonging S-phase, leading to fork collapse and generation of ssDNA regions that are converted to DSBs. These cells continue to proliferate leading to propagation of the DNA damage. This bypassing of DNA repair is consistent with our data that, in the absence of caspase-2, the time between cell divisions is not increased in response to mild DNA damage and that chromosomal damage is not repaired prior to mitosis. Overall, our data indicates an essential role for caspase-2 in the response to DNA damage during cell division.

During cell division, caspase-2 is subject to two separate phosphorylation events that are reported to attenuate its activation downstream of activation platform assembly. These phosphorylation events are induced by Cdk-cyclin B1 and Aurora B kinase at S340 and S384 respectively.^{76, 77} Cdk-cyclin B1 is required for G2/M transition,⁷⁸ while Aurora B kinase is a spindle checkpoint protein and is essential for the segregation of chromosomes.⁷⁹ It has been proposed that these inhibitory phosphorylation events are to prevent caspase-2 from inducing apoptosis during cell division, a process referred to as mitotic catastrophe.^{76, 77} However, we noted that caspase-2 activation in dividing cells was primarily in G1-phase rather than G2, indicating that this is a separate event. In addition, while we noted a strong association between caspase-2 activation and cell division, we did not observe a similar association with cell death. This demonstrates that apoptosis is not the primary outcome of this caspase-2 activation during cell division. Therefore, it is possible that an alternative function of these phosphorylation events is to fine tune caspase-2 activation during different stages of the cell cycle, allowing its activation during G1-phase and downregulating its activity during G2/M.

Treatment with inducers of G2/M arrest including nocodazole and Plk1 inhibition has been shown to induce caspase-2-dependent apoptosis as a mechanism to remove aneuploid cells.⁶⁰ This would suggest that caspase-2 regulates cell cycle during the DNA damage response through activation of the same pathway components that are involved in caspase-2-dependent apoptosis. Arguing against this, our evidence indicates that the cell cycle effects associated with the loss of caspase-2 are not phenocopied by Bcl-X_L overexpression. Bcl-X_L is an effective inhibitor of caspase-2-induced apoptosis via its ability to block the caspase-2 substrate BID and to inhibit mitochondrial outer membrane permeabilization.⁸⁰ This indicates that the cell cycle functions of caspase-2 leading to DNA fork protection and prevention of DNA damage are not simply due to the removal of damaged cells by caspase-2-dependent apoptosis. Our evidence further suggests that the regulation of cell cycle by caspase-2 is mechanistically independent of its ability to induce apoptosis. Caspase-2 cleaves MDM2 to increase p53 stabilization in response to Aurora B kinase inhibition.¹¹ This is important for inducing cell cycle arrest in response to cytokinesis failure leading to PIDDosome assembly on supernumerary centrioles.¹² However, while we noted a slight reduction in p53 stabilization, MDM2 cleavage was not detected following induction of replication stress. This indicates that this is a distinct pathway than the one regulated by Aurora B kinase in response to supernumerary centrioles. Given the independence of this pathway from both apoptosis and MDM2 cleavage, these effects likely due to an, as yet, unidentified caspase-2 target. The difference between the cell cycle and apoptotic functions of caspase-2 may be due to the extent of DNA damage. We show that at increasing doses of DNA damaging agents, the impact of caspase-2 on cell cycle is mitigated. Therefore, at high levels of DNA damage caspase-2 may switch from regulating DNA repair to inducing apoptosis.

In contrast to our work, another group showed that PIDD-deficiency is associated with increased recovery from stalled DNA replication forks induced by UV.⁸¹ The difference between the results of the latter study and our results brings into question the requirement of PIDD for the function of caspase-2 in protecting replication forks. We identified the nucleolar PIDDosome comprising of nucleophosmin (NPM1), PIDD, and RAIDD as a major caspase-2 activating complex in response to topoisomerase I inhibitors that produce ssDNA.¹⁹ We showed that inhibition of NPM1 overcomes caspase-2 associated growth arrest.¹⁹ This may suggest that the nucleolar PIDDosome drives the cell cycle-associated events we report here. However, the activation of caspase-2 during cell division in the absence of DNA damage and in the presence of mild DNA damage was generally cytoplasmic. Our prior results indicated that the cytoplasmic complex formed in response to DNA damage is PIDD independent.¹⁹ Therefore, the cytoplasmic complex may be responsible for the observations we have made here. This provides strong evidence that the localization of caspase-2 activation platform assembly in the nucleolus, at the centrioles or in the cytoplasm leads to dramatically different functional outcomes. Interestingly, we did identify that DNA damage accelerates G1-associated caspase-2 activation in a caspase-2-dependent fashion. This indicates that caspase-2 forms a higher order complex that recruits additional caspase-2 molecules. A similar cytoplasmic complex has been identified for caspase-8 in response to TRAIL where caspase-8 is the scaffold for FADD and RIPK1 recruitment when caspase activation is blocked.⁸² While caspase-2-associated

tumor suppression and regulation of cell division has been shown to require its catalytic activity,⁸ a non-catalytic contribution of caspase-2 to these functions cannot be ruled out. To fully understand the conditions that lead to caspase-2 activation during cell cycle and how this leads to DNA replication fork protection, further exploration of the complexes that lead to caspase-2 activation in this process will be essential.

In conclusion, our data provide strong evidence for an active role for caspase-2 in ensuring correct cell cycling that does not simply lead to removal of damaged cells by apoptosis. This contributes to the growing body of evidence that caspase-2 engages multiple cellular functions to safeguard against genomic instability and tumor progression.

Supplementary Material

Refer to Web version on PubMed Central for supplementary material.

Acknowledgements

We would like to thank Jennifer Martinez (NIEHS) for careful reading of this manuscript. Funding for this project includes NIH/NIGMS R01GM121389 (LBH), NIH/NCI R21CA256606 (LBH) and NIH/NIGMS T32GM008231 (KEL). This project was supported by the Cytometry and Cell Sorting Core at Baylor College of Medicine with funding from the NIH (P30 AI036211, P30 CA125123, and S10 RR024574) and the expert assistance of J. M. Sederstrom. We would like to acknowledge the Texas Children's Hospital William T. Shearer Center for Human Immunobiology for their generous support for this research and the expert assistance of Rebecca Kairis.

References

1. Boice A, Bouchier-Hayes L (2020). Targeting apoptotic caspases in cancer. *Biochimica et biophysica acta Molecular cell research* 1867: 118688. [PubMed: 32087180]
2. Bouchier-Hayes L (2010). The role of caspase-2 in stress-induced apoptosis. *J Cell Mol Med* 14: 1212–1224. [PubMed: 20158568]
3. Bouchier-Hayes L, Green DR (2012). Caspase-2: the orphan caspase. *Cell Death Differ* 19: 51–57. [PubMed: 22075987]
4. Ho LH, Taylor R, Dorstyn L, Cakouros D, Bouillet P, Kumar S (2009). A tumor suppressor function for caspase-2. *Proc Natl Acad Sci U S A* 106: 5336–5341. [PubMed: 19279217]
5. Puccini J, Shalini S, Voss AK, Gatei M, Wilson CH, Hiwase DK et al. (2013). Loss of caspase-2 augments lymphomagenesis and enhances genomic instability in Atm-deficient mice. *Proc Natl Acad Sci U S A* 110: 19920–19925. [PubMed: 24248351]
6. Terry MR, Arya R, Mukhopadhyay A, Berrett KC, Clair PM, Witt B et al. (2015). Caspase-2 impacts lung tumorigenesis and chemotherapy response in vivo. *Cell Death Differ* 22: 719–730. [PubMed: 25301067]
7. Parsons MJ, McCormick L, Janke L, Howard A, Bouchier-Hayes L, Green DR (2013). Genetic deletion of caspase-2 accelerates MMTV/c-neu-driven mammary carcinogenesis in mice. *Cell Death Differ* 20: 1174–1182. [PubMed: 23645210]
8. Ren K, Lu J, Porollo A, Du C (2012). Tumor-suppressing function of caspase-2 requires catalytic site Cys-320 and site Ser-139 in mice. *J Biol Chem* 287: 14792–14802. [PubMed: 22396545]
9. Tinel A, Tschopp J (2004). The PIDDosome, a protein complex implicated in activation of caspase-2 in response to genotoxic stress. *Science* 304: 843–846. [PubMed: 15073321]
10. Berube C, Boucher LM, Ma W, Wakeham A, Salmena L, Hakem R et al. (2005). Apoptosis caused by p53-induced protein with death domain (PIDD) depends on the death adapter protein RAIDD. *Proc Natl Acad Sci U S A* 102: 14314–14320. [PubMed: 16183742]
11. Oliver TG, Meylan E, Chang GP, Xue W, Burke JR, Humpton TJ et al. (2011). Caspase-2-Mediated Cleavage of Mdm2 Creates a p53-Induced Positive Feedback Loop. *Mol Cell* 43: 57–71. [PubMed: 21726810]

12. Fava LL, Schuler F, Sladky V, Haschka MD, Soratroi C, Eiterer L et al. (2017). The PIDDosome activates p53 in response to supernumerary centrosomes. *Genes Dev* 31: 34–45. [PubMed: 28130345]
13. Baptiste-Okoh N, Barsotti AM, Prives C (2008). A role for caspase 2 and PIDD in the process of p53-mediated apoptosis. *Proc Natl Acad Sci U S A* 105: 1937–1942. [PubMed: 18238895]
14. Lassus P, Opitz-Araya X, Lazebnik Y (2002). Requirement for caspase-2 in stress-induced apoptosis before mitochondrial permeabilization. *Science* 297: 1352–1354. [PubMed: 12193789]
15. Robertson JD, Enoksson M, Suomela M, Zhivotovsky B, Orrenius S (2002). Caspase-2 acts upstream of mitochondria to promote cytochrome c release during etoposide-induced apoptosis. *J Biol Chem* 277: 29803–29809. [PubMed: 12065594]
16. Baptiste-Okoh N, Barsotti A, Prives C (2008). A role for caspase 2 and PIDD in the process of p53-mediated apoptosis. *Proc Natl Acad Sci U S A* 105: 1937–1942. [PubMed: 18238895]
17. Sidi S, Sanda T, Kennedy RD, Hagen AT, Jette CA, Hoffmans R et al. (2008). Chk1 suppresses a caspase-2 apoptotic response to DNA damage that bypasses p53, Bcl-2, and caspase-3. *Cell* 133: 864–877. [PubMed: 18510930]
18. Pan Y, Ren KH, He HW, Shao RG (2009). Knockdown of Chk1 sensitizes human colon carcinoma HCT116 cells in a p53-dependent manner to lidamycin through abrogation of a G2/M checkpoint and induction of apoptosis. *Cancer Biol Ther* 8: 1559–1566. [PubMed: 19502782]
19. Ando K, Parsons MJ, Shah RB, Charendoff CI, Paris SL, Liu PH et al. (2017). NPM1 directs PIDDosome-dependent caspase-2 activation in the nucleolus. *J Cell Biol* 216: 1795–1810. [PubMed: 28432080]
20. Robeson AC, Lindblom KR, Wojton J, Kornbluth S, Matsuura K (2018). Dimer-specific immunoprecipitation of active caspase-2 identifies TRAF proteins as novel activators. *EMBO J* 37.
21. Bouchier-Hayes L, Oberst A, McStay GP, Connell S, Tait SW, Dillon CP et al. (2009). Characterization of cytoplasmic caspase-2 activation by induced proximity. *Mol Cell* 35: 830–840. [PubMed: 19782032]
22. Manzl C, Krumschnabel G, Bock F, Sohm B, Labi V, Baumgartner F et al. (2009). Caspase-2 activation in the absence of PIDDosome formation. *J Cell Biol* 185: 291–303. [PubMed: 19364921]
23. Nitiss J, Wang JC (1988). DNA topoisomerase-targeting antitumor drugs can be studied in yeast. *Proceedings of the National Academy of Sciences* 85: 7501–7505.
24. Goldwasser F, Shimizu T, Jackman J, Hoki Y, O'Connor PM, Kohn KW et al. (1996). Correlations between S and G2 arrest and the cytotoxicity of camptothecin in human colon carcinoma cells. *Cancer Res* 56: 4430–4437. [PubMed: 8813137]
25. Nelson WG, Kastan MB (1994). DNA strand breaks: the DNA template alterations that trigger p53-dependent DNA damage response pathways. *Mol Cell Biol* 14: 1815–1823. [PubMed: 8114714]
26. Saintigny Y, Delacote F, Vares G, Petitot F, Lambert S, Averbek D et al. (2001). Characterization of homologous recombination induced by replication inhibition in mammalian cells. *EMBO J* 20: 3861–3870. [PubMed: 11447127]
27. Gundry MC, Brunetti L, Lin A, Mayle AE, Kitano A, Wagner D et al. (2016). Highly Efficient Genome Editing of Murine and Human Hematopoietic Progenitor Cells by CRISPR/Cas9. *Cell reports* 17: 1453–1461. [PubMed: 27783956]
28. Moreno-Mateos MA, Vejnar CE, Beaudoin JD, Fernandez JP, Mis EK, Khokha MK et al. (2015). CRISPRscan: designing highly efficient sgRNAs for CRISPR-Cas9 targeting in vivo. *Nature methods* 12: 982–988. [PubMed: 26322839]
29. Lapytsko A, Kollarovic G, Ivanova L, Studencka M, Schaber J (2015). FoCo: a simple and robust quantification algorithm of nuclear foci. *BMC Bioinformatics* 16.
30. Krull A, Buchholz T-O & Jug F. (2019). Noise2Void - Learning Denoising from Single Noisy Images. . 2019 Ieee Cvf Conf Comput Vis Pattern Recognit Cvpr 00: 2124–2132.
31. von Chamier L, Laine RF, Jukkala J, Spahn C, Krentzel D, Nehme E et al. (2021). Democratising deep learning for microscopy with ZeroCostDL4Mic. *Nature communications* 12: 2276.

32. Stringer C, Wang T, Michaelos M, Pachitariu M (2021). Cellpose: a generalist algorithm for cellular segmentation. *Nature methods* 18: 100–106. [PubMed: 33318659]
33. Singh M, Hunt CR, Pandita RK, Kumar R, Yang CR, Horikoshi N et al. (2013). Lamin A/C depletion enhances DNA damage-induced stalled replication fork arrest. *Mol Cell Biol* 33: 1210–1222. [PubMed: 23319047]
34. Sharma GG, Hwang KK, Pandita RK, Gupta A, Dhar S, Parenteau J et al. (2003). Human heterochromatin protein 1 isoforms HP1(Hsalph) and HP1(Hsbeta) interfere with hTERT-telomere interactions and correlate with changes in cell growth and response to ionizing radiation. *Mol Cell Biol* 23: 8363–8376. [PubMed: 14585993]
35. Hunt CR, Dix DJ, Sharma GG, Pandita RK, Gupta A, Funk M et al. (2004). Genomic instability and enhanced radiosensitivity in Hsp70.1- and Hsp70.3-deficient mice. *Mol Cell Biol* 24: 899–911. [PubMed: 14701760]
36. Baliga BC, Read SH, Kumar S (2004). The biochemical mechanism of caspase-2 activation. *Cell Death Differ* 11: 1234–1241. [PubMed: 15297885]
37. Nishitani H, Lygerou Z, Nishimoto T (2004). Proteolysis of DNA replication licensing factor Cdt1 in S-phase is performed independently of geminin through its N-terminal region. *J Biol Chem* 279: 30807–30816. [PubMed: 15138268]
38. Sakaue-Sawano A, Kurokawa H, Morimura T, Hanyu A, Hama H, Osawa H et al. (2008). Visualizing spatiotemporal dynamics of multicellular cell-cycle progression. *Cell* 132: 487–498. [PubMed: 18267078]
39. Nishitani H, Taraviras S, Lygerou Z, Nishimoto T (2001). The human licensing factor for DNA replication Cdt1 accumulates in G1 and is destabilized after initiation of S-phase. *J Biol Chem* 276: 44905–44911. [PubMed: 11555648]
40. Bianchi V, Pontis E, Reichard P (1986). Changes of deoxyribonucleoside triphosphate pools induced by hydroxyurea and their relation to DNA synthesis. *Journal of Biological Chemistry* 261: 16037–16042.
41. Singh DK, Pandita RK, Singh M, Chakraborty S, Hambarde S, Ramnarain D et al. (2018). MOF Suppresses Replication Stress and Contributes to Resolution of Stalled Replication Forks. *Mol Cell Biol* 38.
42. Saintigny Y (2001). Characterization of homologous recombination induced by replication inhibition in mammalian cells. *The EMBO Journal* 20: 3861–3870. [PubMed: 11447127]
43. Rogakou EP, Pilch DR, Orr AH, Ivanova VS, Bonner WM (1998). DNA Double-stranded Breaks Induce Histone H2AX Phosphorylation on Serine 139. *Journal of Biological Chemistry* 273: 5858–5868.
44. Mattoo AR, Pandita RK, Chakraborty S, Charaka V, Mujoo K, Hunt CR et al. (2017). MCL-1 Depletion Impairs DNA Double-Strand Break Repair and Reinitiation of Stalled DNA Replication Forks. *Mol Cell Biol* 37.
45. Zou L, Elledge SJ (2003). Sensing DNA damage through ATRIP recognition of RPA-ssDNA complexes. *Science* 300: 1542–1548. [PubMed: 12791985]
46. Sanchez Y (1997). Conservation of the Chk1 Checkpoint Pathway in Mammals: Linkage of DNA Damage to Cdk Regulation Through Cdc25. *Science* 277: 1497–1501. [PubMed: 9278511]
47. Mailand N (2000). Rapid Destruction of Human Cdc25A in Response to DNA Damage. *Science* 288: 1425–1429. [PubMed: 10827953]
48. Liu S, Shiotani B, Lahiri M, Marechal A, Tse A, Leung CC et al. (2011). ATR autophosphorylation as a molecular switch for checkpoint activation. *Mol Cell* 43: 192–202. [PubMed: 21777809]
49. Falck J, Petrini JHJ, Williams BR, Lukas J, Bartek J (2002). The DNA damage-dependent intra-S phase checkpoint is regulated by parallel pathways. *Nature Genetics* 30: 290–294. [PubMed: 11850621]
50. Matsuoka S, Huang M, Elledge SJ (1998). Linkage of ATM to cell cycle regulation by the Chk2 protein kinase. *Science* 282: 1893–1897. [PubMed: 9836640]
51. Ismail IH, Nyström S, Nygren J, Hammarsten O (2005). Activation of Ataxia Telangiectasia Mutated by DNA Strand Break-inducing Agents Correlates Closely with the Number of DNA Double Strand Breaks. *Journal of Biological Chemistry* 280: 4649–4655.

52. Guo Y, Srinivasula SM, Druilhe A, Fernandes-Alnemri T, Alnemri ES (2002). Caspase-2 induces apoptosis by releasing proapoptotic proteins from mitochondria. *J Biol Chem* 277: 13430–13437. [PubMed: 11832478]
53. Bonzon C, Bouchier-Hayes L, Pagliari LJ, Green DR, Newmeyer DD (2006). Caspase-2-induced apoptosis requires bid cleavage: a physiological role for bid in heat shock-induced death. *Mol Biol Cell* 17: 2150–2157. [PubMed: 16495337]
54. Howard A (1953). Synthesis of deoxyribonucleic acid in normal and irradiated cells and its relation to chromosome breakage. *Heredity Suppl* 6: 261–273.
55. Kuzminov A (1995). Collapse and repair of replication forks in *Escherichia coli*. *Molecular microbiology* 16: 373–384. [PubMed: 7565099]
56. Zeman MK, Cimprich KA (2014). Causes and consequences of replication stress. *Nat Cell Biol* 16: 2–9. [PubMed: 24366029]
57. Bester AC, Roniger M, Oren YS, Im MM, Sami D, Chaoat M et al. (2011). Nucleotide deficiency promotes genomic instability in early stages of cancer development. *Cell* 145: 435–446. [PubMed: 21529715]
58. Beck H, Nahse-Kumpf V, Larsen MS, O’Hanlon KA, Patzke S, Holmberg C et al. (2012). Cyclin-dependent kinase suppression by WEE1 kinase protects the genome through control of replication initiation and nucleotide consumption. *Mol Cell Biol* 32: 4226–4236. [PubMed: 22907750]
59. Lopez-Garcia C, Sansregret L, Domingo E, McGranahan N, Hobor S, Birkbak NJ et al. (2017). BCL9L Dysfunction Impairs Caspase-2 Expression Permitting Aneuploidy Tolerance in Colorectal Cancer. *Cancer cell* 31: 79–93. [PubMed: 28073006]
60. Dawar S, Lim Y, Puccini J, White M, Thomas P, Bouchier-Hayes L et al. (2017). Caspase-2-mediated cell death is required for deleting aneuploid cells. *Oncogene* 36: 2704–2714. [PubMed: 27991927]
61. Paulovich AG, Hartwell LH (1995). A checkpoint regulates the rate of progression through S phase in *S. cerevisiae* in response to DNA damage. *Cell* 82: 841–847. [PubMed: 7671311]
62. Byun TS, Pacek M, Yee MC, Walter JC, Cimprich KA (2005). Functional uncoupling of MCM helicase and DNA polymerase activities activates the ATR-dependent checkpoint. *Genes Dev* 19: 1040–1052. [PubMed: 15833913]
63. Blackford AN, Jackson SP (2017). ATM, ATR, and DNA-PK: The Trinity at the Heart of the DNA Damage Response. *Mol Cell* 66: 801–817. [PubMed: 28622525]
64. Saldivar JC, Cortez D, Cimprich KA (2017). The essential kinase ATR: ensuring faithful duplication of a challenging genome. *Nature Reviews Molecular Cell Biology* 18: 622–636. [PubMed: 28811666]
65. Wang H, Wang H, Powell SN, Iliakis G, Wang Y (2004). ATR affecting cell radiosensitivity is dependent on homologous recombination repair but independent of nonhomologous end joining. *Cancer Res* 64: 7139–7143. [PubMed: 15466211]
66. Couch FB, Bansbach CE, Driscoll R, Luzwick JW, Glick GG, Betous R et al. (2013). ATR phosphorylates SMARCAL1 to prevent replication fork collapse. *Genes Dev* 27: 1610–1623. [PubMed: 23873943]
67. Ceccaldi R, Sarangi P, D’Andrea AD (2016). The Fanconi anaemia pathway: new players and new functions. *Nat Rev Mol Cell Biol* 17: 337–349. [PubMed: 27145721]
68. Abraham RT (2001). Cell cycle checkpoint signaling through the ATM and ATR kinases. *Genes & Development* 15: 2177–2196. [PubMed: 11544175]
69. Khanna KK, Keating KE, Kozlov S, Scott S, Gatei M, Hobson K et al. (1998). ATM associates with and phosphorylates p53: mapping the region of interaction. *Nature Genetics* 20: 398–400. [PubMed: 9843217]
70. Gatei M, Scott SP, Filippovitch I, Soronika N, Lavin MF, Weber B et al. (2000). Role for ATM in DNA damage-induced phosphorylation of BRCA1. *Cancer Res* 60: 3299–3304. [PubMed: 10866324]
71. Lim D-S, Kim S-T, Xu B, Maser RS, Lin J, Petrini JHJ et al. (2000). ATM phosphorylates p95/nbs1 in an S-phase checkpoint pathway. *Nature* 404: 613–617. [PubMed: 10766245]

72. Matsuoka S, Rotman G, Ogawa A, Shiloh Y, Tamai K, Elledge SJ (2000). Ataxia telangiectasia-mutated phosphorylates Chk2 in vivo and in vitro. *Proceedings of the National Academy of Sciences* 97: 10389–10394.
73. Chaturvedi P, Eng WK, Zhu Y, Mattern MR, Mishra R, Hurler MR et al. (1999). Mammalian Chk2 is a downstream effector of the ATM-dependent DNA damage checkpoint pathway. *Oncogene* 18: 4047–4054. [PubMed: 10435585]
74. Brown AL, Lee CH, Schwarz JK, Mitiku N, Piwnicka-Worms H, Chung JH (1999). A human Cds1-related kinase that functions downstream of ATM protein in the cellular response to DNA damage. *Proceedings of the National Academy of Sciences* 96: 3745–3750.
75. Zhong Y, Nellimoottil T, Peace JM, Knott SR, Villwock SK, Yee JM et al. (2013). The level of origin firing inversely affects the rate of replication fork progression. *J Cell Biol* 201: 373–383. [PubMed: 23629964]
76. Andersen JL, Johnson CE, Freeland CD, Parrish AB, Day JL, Buchakjian MR et al. (2009). Restraint of apoptosis during mitosis through interdomain phosphorylation of caspase-2. *Embo J*.
77. Lim Y, De Bellis D, Sandow JJ, Capalbo L, D'Avino PP, Murphy JM et al. (2020). Phosphorylation by Aurora B kinase regulates caspase-2 activity and function. *Cell Death Differ*.
78. Nurse P (1990). Universal control mechanism regulating onset of M-phase. *Nature* 344: 503–508. [PubMed: 2138713]
79. Glover DM, Leibowitz MH, McLean DA, Parry H (1995). Mutations in aurora prevent centrosome separation leading to the formation of monopolar spindles. *Cell* 81: 95–105. [PubMed: 7720077]
80. Gao Z, Shao Y, Jiang X (2005). Essential roles of the Bcl-2 family of proteins in caspase-2-induced apoptosis. *J Biol Chem* 280: 38271–38275. [PubMed: 16172118]
81. Lin Y-F, Shih H-Y, Shang Z-F, Kuo C-T, Guo J, Du C et al. (2018). PIDD mediates the association of DNA-PKcs and ATR at stalled replication forks to facilitate the ATR signaling pathway. *Nucleic Acids Research* 46: 1847–1859. [PubMed: 29309644]
82. Henry CM, Martin SJ (2017). Caspase-8 Acts in a Non-enzymatic Role as a Scaffold for Assembly of a Pro-inflammatory “FADDosome” Complex upon TRAIL Stimulation. *Mol Cell* 65: 715–729 e715. [PubMed: 28212752]

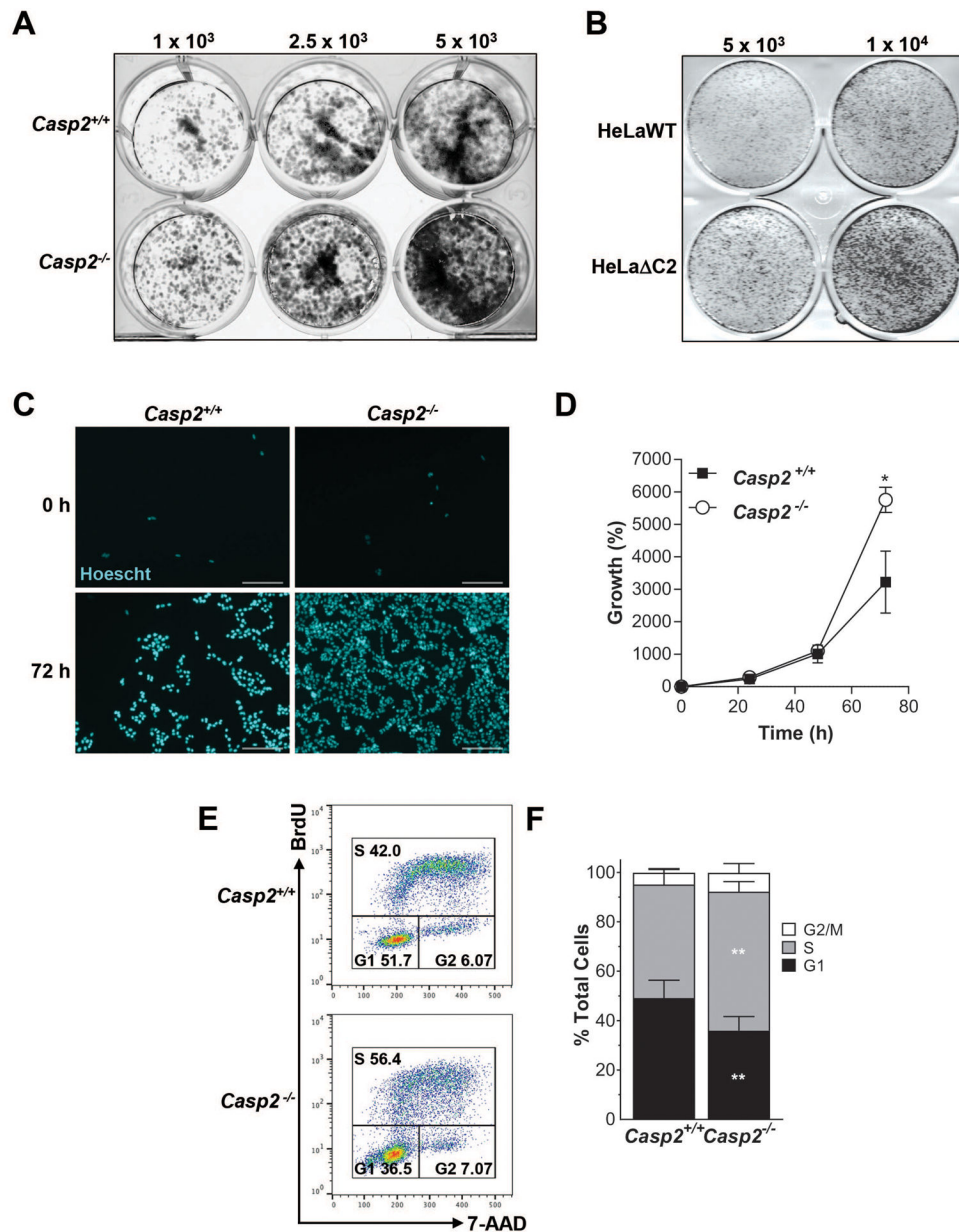


Figure 1. Caspase-2 limits cellular proliferation.

(A) Litter-matched *Casp2*^{+/+} and *Casp2*^{-/-}E1A/Ras transformed mouse embryonic fibroblasts (MEF) were plated at the indicated cell number. Viable cells were stained with methylene blue 4 days after plating. Representative images of methylene blue-stained colonies are shown from three independent experiments. (B) Wild type (WT) or CRISPR/Cas9 generated caspase-2 deficient (Δ C2) HeLa cells were plated at the indicated cell number. Viable cells were stained with methylene blue 4 days after plating. Representative images of methylene blue-stained colonies are shown from three independent experiments. (C) Litter-matched *Casp2*^{+/+} and *Casp2*^{-/-} E1A/Ras transformed MEF, plated at low density, were stained with Hoechst 33342 and imaged at the indicated time points. Representative images are shown from the 0 h and 72 h time points. Nuclei are shown in blue. Bar,

200 μm . **(D)** Total number of cells from (C) was determined by counting Hoechst-positive cells from at least 30 images per well. Results are shown as the percent increase in cell growth compared to 0 h and are the average of three independent experiments plus or minus standard deviation. * $p < 0.05$. **(E)** Untreated, cycling litter-matched *Casp2*^{+/+} and *Casp2*^{-/-} E1A/Ras MEF were stained with anti-BrdU-FITC/7-AAD and analyzed by flow cytometry. Representative flow plots are shown. **(F)** The percentage of cells in G1, S, or G2/M phase for each cell line is shown. Results are the average of seven independent experiments plus or minus standard deviation. ** $p < 0.01$.

Author Manuscript

Author Manuscript

Author Manuscript

Author Manuscript

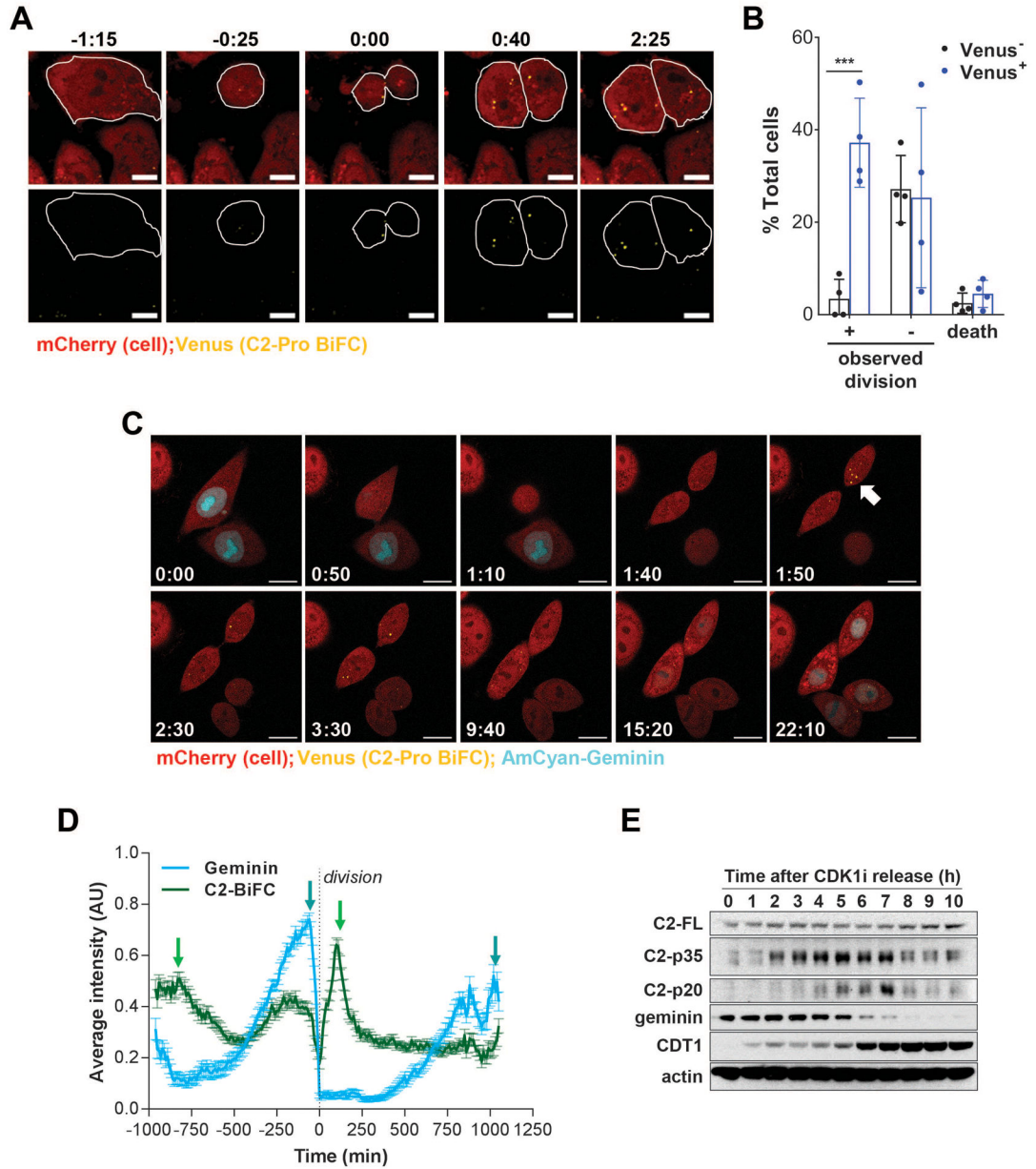


Figure 2. Caspase-2 is activated in dividing cells.

(A) HeLa cells stably expressing C2 Pro-VC-2A-C2 Pro-VN-2A-mCherry (HeLa.C2 Pro-BiFC) were imaged every 5 min for 16 h. Representative sequential images show the appearance of caspase-2 BiFC (*yellow*) in dividing cells (*red*). (B) The percentage of mCherry-positive cells that became Venus-positive or remained Venus-negative were categorized into those with observed division, no observed division, or observed cell death within the 16 h time-lapse. At least 100 cells per experiment were measured. Results are the average of four independent experiments (represented by symbols) plus or minus standard deviation. *** $p < 0.001$. (C) HeLa.C2 Pro-BiFC cells stably expressing AmCyan-Geminin were imaged every 10 min for 24 h. Frames from the time-lapse show representative cells undergoing BiFC (*yellow*) relative to geminin expression as measured by Cyan fluorescence

(*blue*). Scale bars represent 10 μm . **(D)** Graph of the dividing cells that became Venus-positive and Cyan-positive is shown. Each point on the Cyan graph (*blue*) is scaled and aligned to each point on the caspase-2 BiFC graph (*green*) that represents the average intensity of Cyan or Venus respectively in the cell at 10 min intervals where time=0 is the time of cell division, as measured by a reduction in cell area (not shown). The peaks of Cyan intensity (*blue arrows*) represents G2-phase of the cell cycle and the peaks of Venus intensity represent caspase-2 activation as measured by BiFC (*green arrows*). Error bars represent SEM of 94 individual cell divisions. **(E)** HeLa cells were synchronized in G2 by double thymidine block followed by inhibition of CDK1 using Ro-3306 (CDK1i). Lysates were collected every hour after the removal of CDK1i and immunoblotted for the indicated proteins.

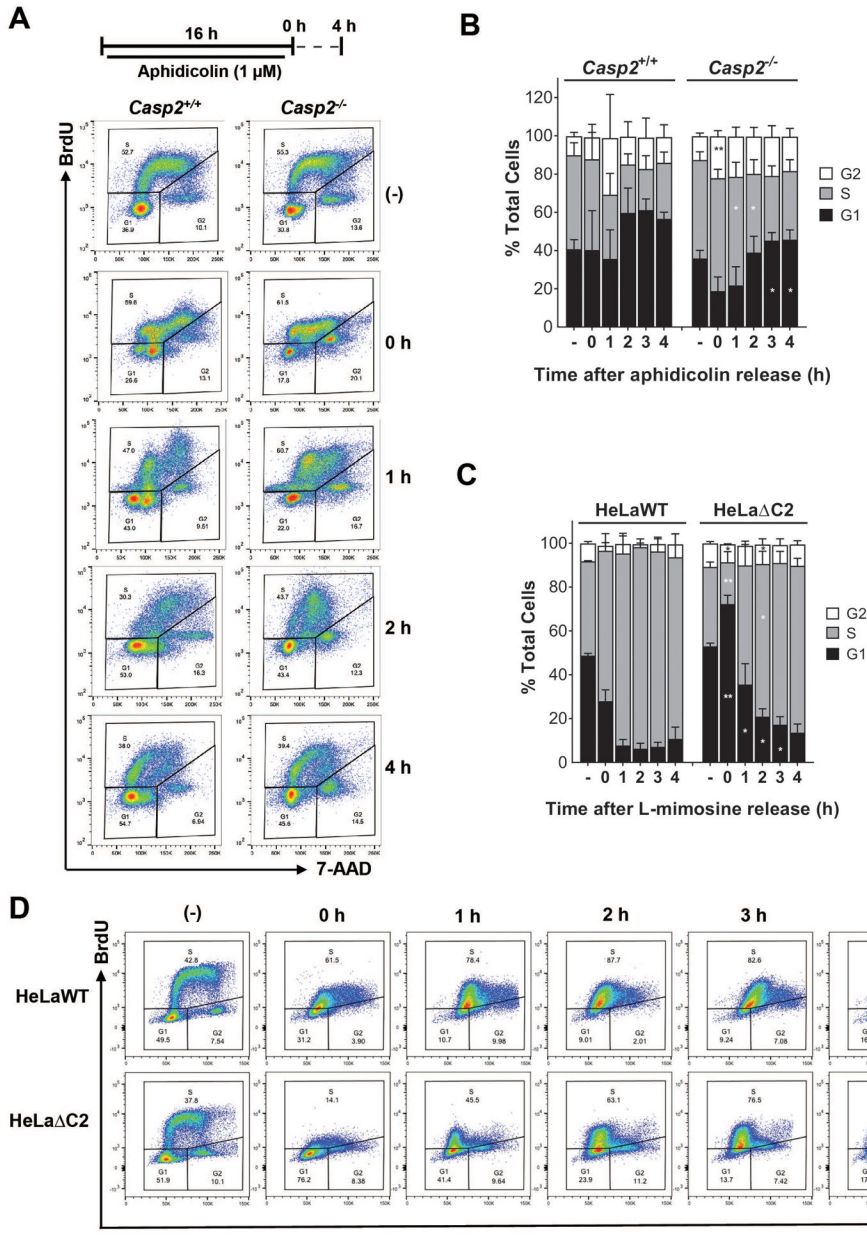


Figure 3. Loss of caspase-2 results in delayed exit from S-Phase following arrest. (A) Litter-matched *Casp2*^{+/+} and *Casp2*^{-/-} E1A/Ras transformed MEF were either left untreated (-) or treated with aphidicolin (1 μ M). After 16 h, the treatment was removed and replaced with fresh media (0 h). Cells were harvested following a 30 min BrdU (10 μ M) pulse at the indicated time points after aphidicolin release and stained with anti-BrdU-FITC/7-AAD as shown in the experimental scheme (*upper panel*). The proportion of cells in S-, G1- and G2-phase was determined by flow cytometry. Representative flow plots are shown (*lower panel*). (B) The percent of cells in each phase of the cell cycle was determined for each time point following aphidicolin release. Results are the average of 5 independent experiments plus or minus standard deviation. *p<0.05. (C) HeLaWT or HeLa Δ C2 cells were treated with L-mimosine (0.5 mM) for 24 h. L-mimosine was removed and cells were

stained with anti-BrdU-FITC/7-AAD and analyzed as in (A). The percent of cells in each phase of the cell cycle was determined for each time point following L-mimosine release. Results are the average of 3 independent experiments plus or minus standard deviation. * $p < 0.05$, ** $p < 0.01$. **(D)** Representative flow plots from (C) are shown.

Author Manuscript

Author Manuscript

Author Manuscript

Author Manuscript

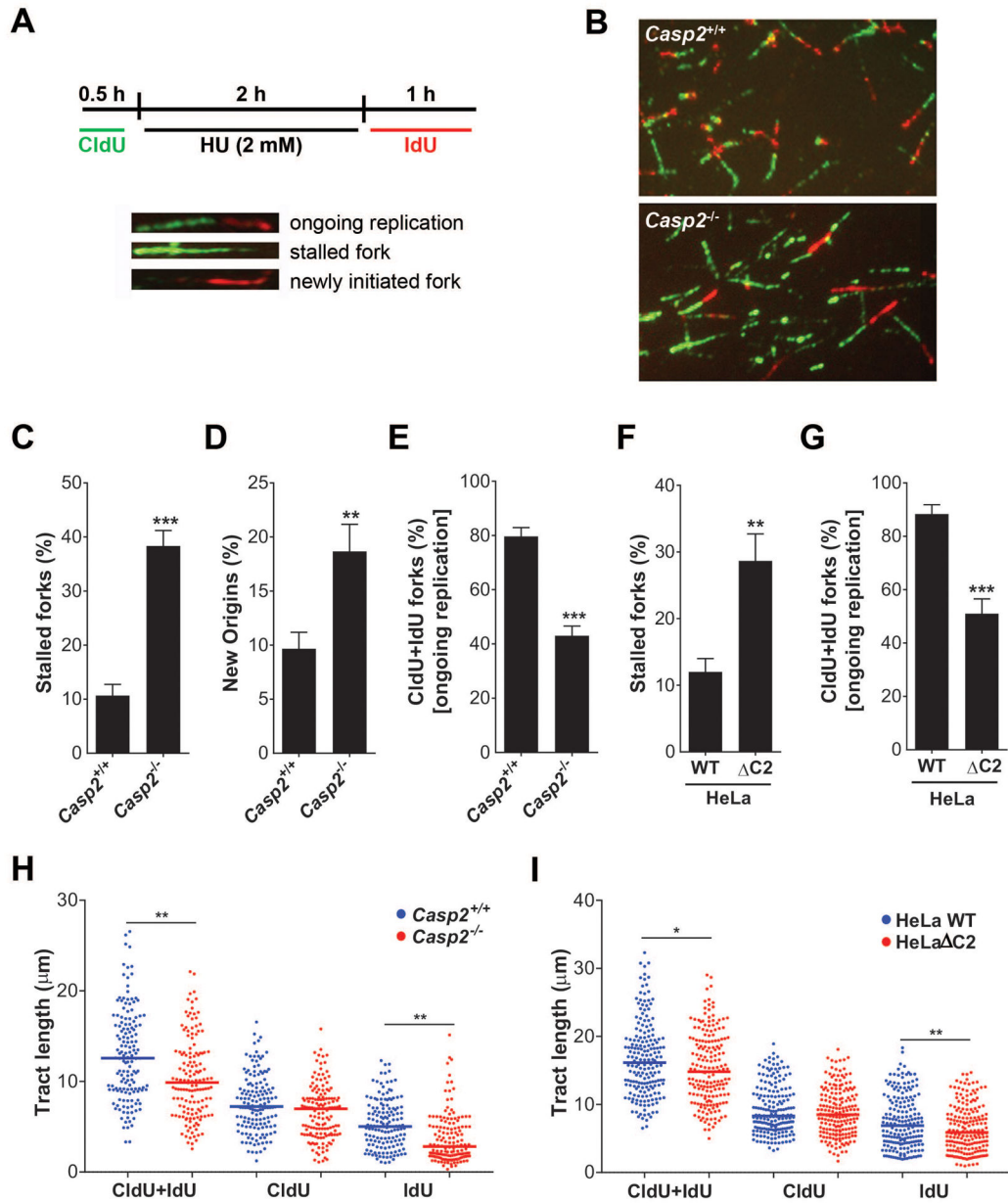


Figure 4. Loss of caspase-2 is associated with stalled replication forks.

(A) Scheme for dual labeling of DNA fibers to evaluate replication restart or recovery following HU-induced replication fork stalling. (B) Representative images of replication tracts from litter-matched *Casp2^{+/+}* and *Casp2^{-/-}* E1A/Ras-transformed MEF after HU treatment showing CldU (5-chloro-2'-deoxyuridine, green) and IdU (5-iodo-2'-deoxyuridine, red) labeled tracts are shown. (C to E). Quantitative analysis of the DNA fiber replication restart assay after HU treatment shows the percentage of stalled forks (C), new origins (D), and total tracts with both CldU and IdU labels at the fork (CldU+IdU) (E) in *Casp2^{+/+}* and *Casp2^{-/-}* MEF; stalled forks (F), and total tracts (CldU+IdU) (G) in HeLa WT and HeLa Δ C2 cells; and tract lengths in MEF (H) and HeLa cells (I) of the indicated genotype. About 300 fibers were analyzed for each condition. * $p < 0.05$, ** $p < 0.01$, *** $p < 0.001$.

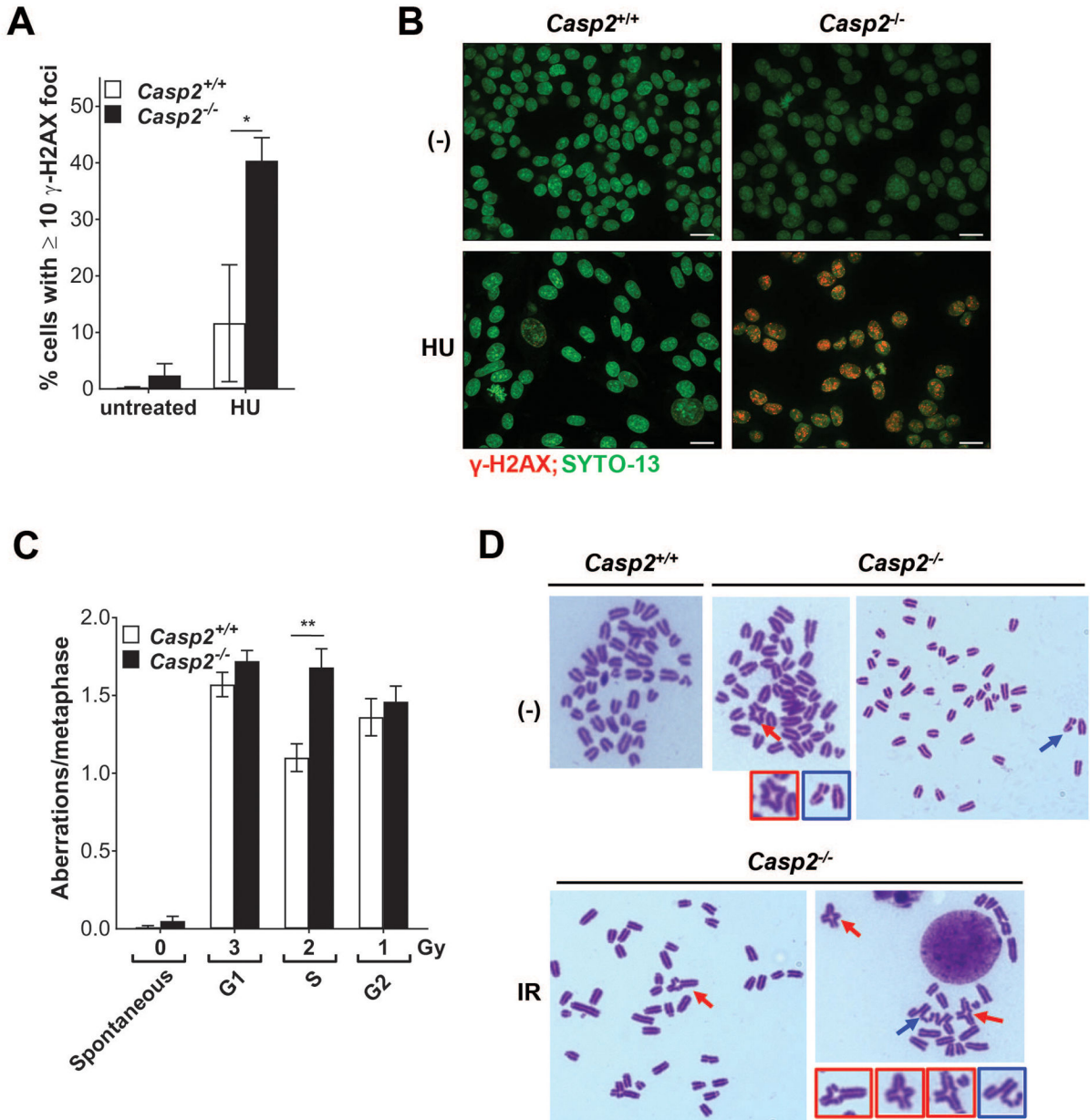


Figure 5: Loss of caspase-2 is associated with increased DNA damage and impaired DNA repair. (A) *Casp2*^{+/+} and *Casp2*^{-/-} MEF treated with DMSO or HU (2 mM) for 2 h followed by recovery for 24 h were stained for γ-H2AX. γ-H2AX foci were counted per cell and the percentage of cells with ≥ 10 foci was calculated from at least 30 images per treatment. Results are the average of three independent experiments plus or minus standard deviation. *p<0.05. (B) Representative images from (A) are shown as maximum intensity projections of 5 image Z stacks, with nuclei shown in green and γ-H2AX foci in red. Bar, 50 μm. (C) Litter-matched *Casp2*^{+/+} and *Casp2*^{-/-} E1A/Ras transformed MEF in exponential phase were treated with the indicated doses of γ-irradiation and were grown until metaphase (10 h for G1, 4 h for S and 1 h for G2). Metaphase spreads were prepared and analyzed for chromosomal aberrations that included chromosome and chromatid type breaks and fusions.

A total of 35 metaphases were analyzed from each sample and the experiment was repeated three times. ****p<0.01. (D)** Representative images of metaphase spread of untreated (–) *Casp2*^{+/+}, *Casp2*^{-/-} and irradiated *Casp2*^{-/-} MEF. Blue arrows show breaks; red arrows show exchanges/radials. Insets show zoomed in images of breaks (*blue boxes*) and radials (*red boxes*).

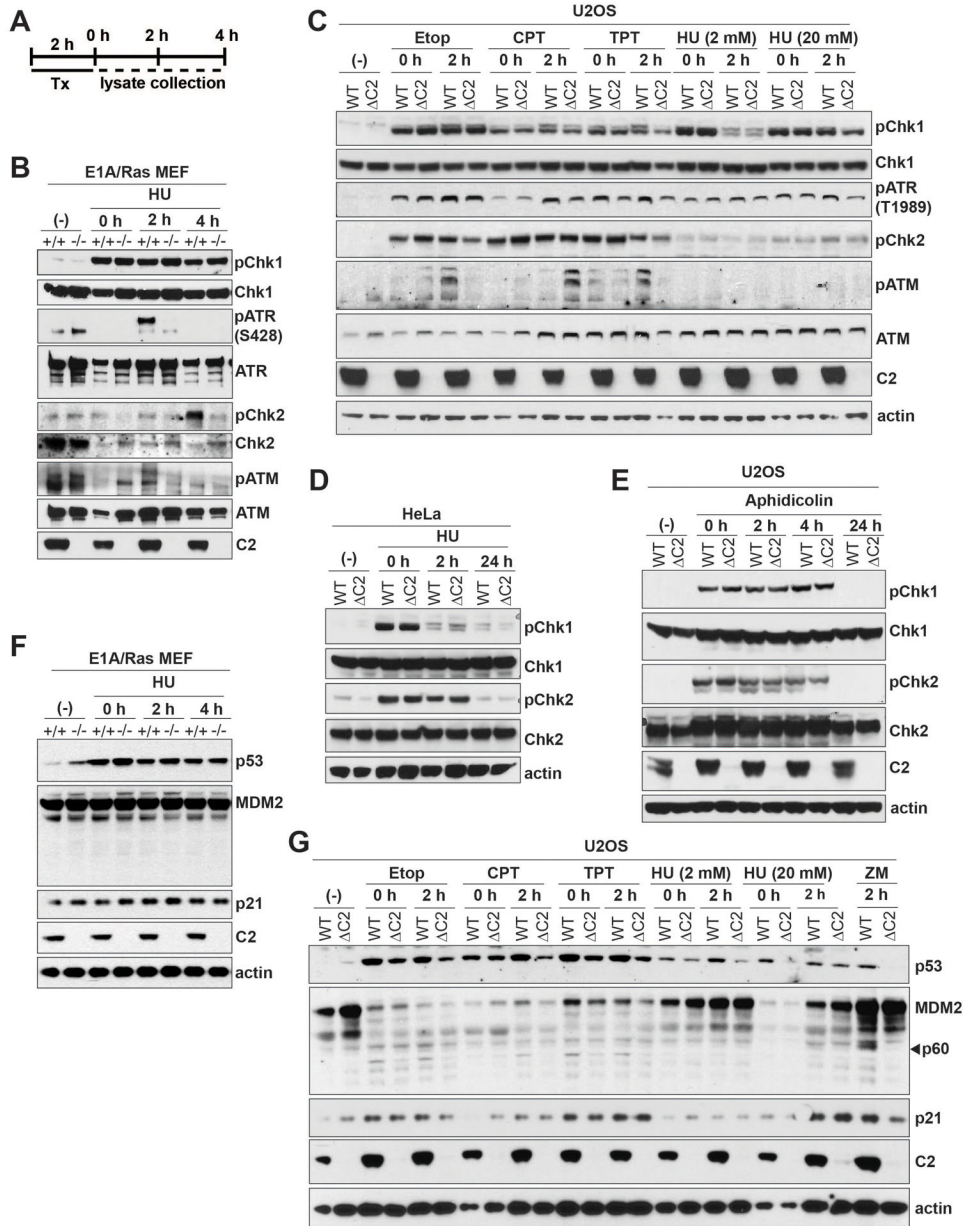


Figure 6. The impact of caspase-2 loss on cell cycle checkpoints.

(A) Scheme for treatment and lysate harvest to evaluate checkpoint analysis following cell cycle arrest or DNA damage (Tx). (B) Litter-matched *Casp2*^{+/+} and *Casp2*^{-/-} E1A/Ras-transformed MEF were either left untreated (-) or treated with hydroxyurea (HU, 2 mM) for 2 h followed by replacement with fresh media (0 h). Cells were harvested at the indicated time points following removal of HU. Cell lysates were immunoblotted for the indicated checkpoint proteins and their phosphorylated counterparts. (C) U2OS cells (WT) or CRISPR/Cas9-generated caspase-2-deficient U2OS cells (C2) were left untreated or treated with etoposide (20 μM), camptothecin (100 μM), topotecan (100 μM) for 4 h, or with HU (2 mM or 20 mM) for 2 h followed by replacement with fresh media (0 h). Cells were harvested at the indicated time points following removal of the drug and lysates were

immunoblotted for the indicated proteins. **(D)** HeLaWT or HeLa C2 cells were treated as in (B). Lysates were immunoblotted for the indicated proteins. **(E)** U2OSWT or U2OS C2 cells were treated with aphidicolin (1 μ M) for 16 h followed by replacement with fresh media. Cells were harvested at the indicated times and lysates were immunoblotted for the indicated proteins. **(F)** Litter-matched *Casp2*^{+/+} and *Casp2*^{-/-} E1A/Ras-transformed MEF were treated as in (B) and cell lysates were immunoblotted for the indicated proteins. **(G)** U2OSWT or U2OS C2 cells were treated as in (C) or with ZM447439 (ZM, 2 μ M). Lysates were immunoblotted for the indicated proteins. Each experiment is representative of 2–6 independent experiments. Actin was used as a loading control.

Author Manuscript

Author Manuscript

Author Manuscript

Author Manuscript

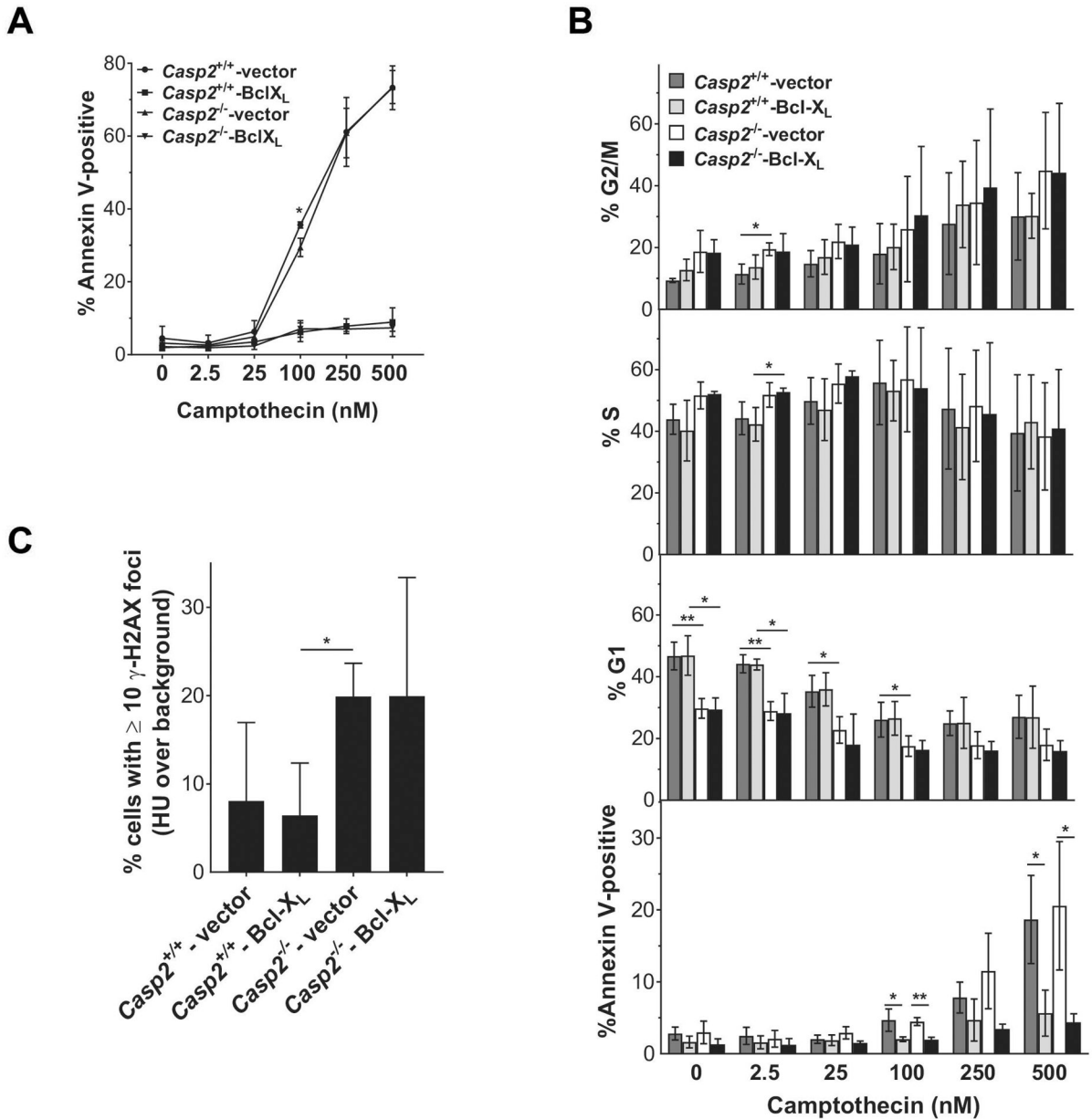


Figure 7. The role of caspase-2 in cell division is independent of its ability to induce apoptosis. (A) Litter-matched *Casp2*^{+/+} and *Casp2*^{-/-} E1A/Ras transformed MEF stably expressing vector or Bcl-X_L were treated with the indicated doses of camptothecin for 24 h. Apoptosis was measured by flow cytometry for Annexin V staining. (B) Cycling *Casp2*^{+/+} and *Casp2*^{-/-} MEF stably expressing vector or Bcl-X_L were left untreated or were treated with the indicated doses of camptothecin for 4 h. Cells were harvested following a 30 min BrdU (10 μM) pulse and stained with anti-BrdU-FITC/7-AAD to determine the percentage of cells in G1-, S- or G2/M-phase of the cell cycle. Apoptosis, as measured by Annexin V staining at 24 h, is shown in the lower panel. Results are the average of 3 independent experiments plus or minus standard deviation. (C) *Casp2*^{+/+} and *Casp2*^{-/-} MEF stably expressing vector or Bcl-X_L treated with DMSO or HU (2 mM) for 2 h followed by recovery for 24 h were

stained for γ -H2AX. γ -H2AX foci were counted per cell and the percentage of cells with 10 foci/cell was calculated from at least 30 images per treatment. Results are shown as % cells with 10 foci/cell above untreated for each genotype. The average of three independent experiments plus or minus standard deviation is shown. * $p < 0.05$; ** $p < 0.01$.

Author Manuscript

Author Manuscript

Author Manuscript

Author Manuscript

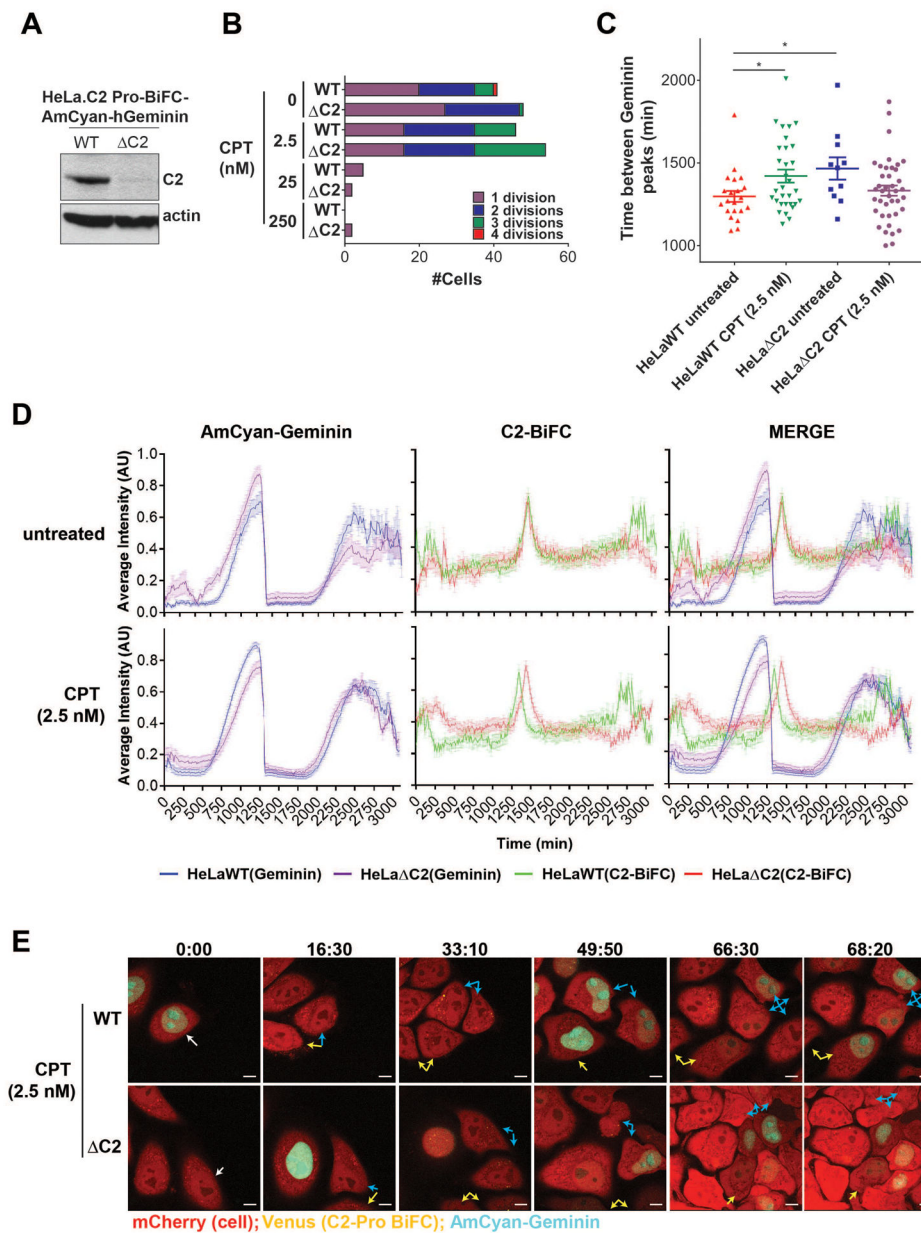


Figure 8: Loss of caspase-2 leads to faster recovery from mild DNA damage.

(A) HeLa.C2 Pro-BiFC AmCyan-hGeminin cells that were wild type (WT) or caspase-2 deficient as generated by CRISPR/Cas9 (ΔC2) were immunoblotted for caspase-2 with actin as a loading control. (B) HeLa.C2 Pro-BiFC AmCyan-hGeminin WT or ΔC2 cells were treated with the indicated amounts of camptothecin (CPT). Cells were imaged every 10 min for 48 h. The total number of cell divisions per founder cell in the 68.5 h time-lapse is shown for the indicated cell types and treatments. (C) The time between the highest point of subsequent geminin peaks representing a full cell cycle is shown for the indicated cell types and treatments. Error bars represent SEM. * $p < 0.05$. (D) The kinetics of cell division compared to caspase-2 BiFC is shown. Each point on the graph represents the average intensity of AmCyan-Geminin (blue and purple traces) or Venus (C2-BiFC, red and green

traces) in the cells at 10 min intervals aligned to the point of cell division, as measured by a reduction in cell area (not shown). Cells that did not divide, died or did not induce BiFC were excluded. Error bars represent SEM of 22 (WT untreated), 34 (WT CPT), 24 (C2 untreated) and 42 (C2) individual cell divisions. **(E)** Frames from the time-lapse show representative HeLa.C2-ProBiFC.AmCyan-hGeminin WT or C2 cells undergoing cell division. Cells show C2-BiFC (*yellow*), geminin expression (*cyan*) and mCherry (*red*) is expressed throughout the cell. White arrows indicate founders and yellow and blue arrows indicate the daughter cells and their progeny. Scale bars represent 10 μm .